Fall 2021

Mathematical Model for SEI Growth Under Open-Circuit Conditions

Wei Shang

Mathematical Model for SEI Growth under Open-circuit Conditions

by

Wei Shang

Bachelor of Engineering
Shenyang Aerospace University, 2018

Submitted in Partial Fulfillment of the Requirements

For the Degree of Master of Science in

Chemical Engineering

College of Engineering and Computing

University of South Carolina

2021

Accepted by:

Ralph White, Director of Thesis

Melissa Moss, Reader

Edward Gatzke, Reader

James Ritter, Reader

Tracey L. Weldon, Interim Vice Provost and Dean of the Graduate School

ACKNOWLEDGMENT

I would like to acknowledge Dr. White for his consistent leadership. I appreciate that I learned a lot from his course. I also greatly appreciate my fellow research group members, Dr. Coman, Dr. Niloofar, Shiv Krishna Madi Reddy, Dave, and Dani. Without their help and support along the way, it is hard for me to finish this project.

I would also like to thank my committee members: Dr. Melissa Moss, Dr. James Ritter and Dr. Edward Gatzke for their insightful comments and encouragement.

I am very thankful to my friend, Cheng Yu. He helps me some technical problems. My roommates, Weiguang Jia, he is graduated student and helps me some knowledge about how to work on thesis. Besides, Yibing Zhang, although she is not here, she gave me a lot of suggestions when I met trouble on the project.

ABSTRACT

An irreversible capacity loss will take place in lithium ions batteries due to the solid electrolyte interface (SEI) creating, which consumes the active lithium and reduces solvent. SEI is either good since it can prevent further electrolyte decomposition or bad for lessening batteries' lifetime. Mathematical modeling of SEI formation is done within a porous electrode to model an empirical battery in the x-direction.

A solid electrolyte interphase (SEI) growth model is developed in a mixed mode which contains solvent diffusion through the SEI layer and its corresponding kinetics of solvent reduction at the electrode surface. The governing equations are numerically solved by the Landau transformation, which makes the moving layer fixed and predicts the open circuit potential, SEI film thickness, and capacity loss. The estimated parameters fitted with experimental data in the literature are computed by COMSOL and MATLAB in this work. Results show that the mixed mode model predicts less capacity loss and thinner SEI thickness due to the growth of the SEI film under open circuit conditions than previously reported by others.

Keywords: SEI layer, mixed-mode, open circuit, mathematical simulation, Landau transformation

TABLE OF CONTENT

LIST OF TABLES

LIST OF FIGURES

LIST OF SYMBOLS

a	Specific surface area
c_{Li}	Lithium ions concentration (mol/m^3)
$c_{Li,max}$	Maximum lithium ions concentration (mol/m^3)
c_s	Solvent concentration in the SEI layer (mol/m^3)
$c_{s,bulk}$	Bulk solution of solvent (mol/m^3)
c_p	Concentration of product (mol/m^3)
D_s	Diffusion coefficient of solvent (m^2/s)
D_s^{eff}	Effective diffusion coefficient of solid lithium (m^2/s)
F	Faraday's constant $96485\ C/mol$
J_{SEI}	Current density of SEI formation(A/m^2)
k_{SEI}	Reaction rate of SEI formation (m/s)
L	SEI thickness (nm)
n	The number of transferred electrons
Q	Capacity loss $(\mu Ah/cm^2)$
R	Gas constant, 8.314 J/mol K
T	Absolute temperature (K)
U^{OCP}	Equilibrium potential of negative electrode (V)
U_s^{SEI}	Equilibrium potential of the solvent reduction reaction (V)
α	Transfer coefficient for solvent reduction reaction

ε_{SEI}	Porosity of the SEI layer
η_{SEI}	Overpotential for solvent reduction reaction (V)

LIST OF ABBREVIATIONS

AM .... Active Material

DEC...Diethyl carbonate

DMC ....Dimethyl carbonate

EC ....Ethylene carbonate

ICL ....Irreversible capacity loss

LIB .... Lithium ions batteries

OCV ....Open circuit voltage

RCL..Reversible capacity loss

SEI.. Solid electrolyte interface

SOC...State of charge

CHAPTER 1

INTRODUCTION

Lithium ions batteries (LIB) are widely used in smartphones, laptops, electric vehicles since its high energy density. LIB's safety by applying graphite as the negative electrode is increasing, whose capacity is much lower than Li metal[1], carbon material might induce side reaction because it is a place where electrons and lithium ions are combined and then stored through intercalation. During the first charge of a lithium-ion battery, the electrolyte undergoes a reduction on the negative graphite electrode's surface. This reduction is supposed to cease LIB's performance as a passivating layer generates on the negative electrode[2-7]. Peled[5] named it a solid electrolyte interface (SEI). Around SEI, I will elaborate on this project.

1.1 SEI mechanism and properties

During the lithiation of the graphite electrode of lithium ions battery, the potential of the electrode will decrease, then the electrolyte decomposition product are forming an SEI layer[3]. This new phase grows between the electrode and electrolyte. The growth of SEI layer relies on the solvent reduction reaction with deintercalated lithium ions from negative graphite electrode and electrons. Yang et al.[8] investigated only ethylene carbonate (EC) decompose in EC/ diethyl carbonate (DEC) or EC/ dimethyl carbonate (DMC) binary solvent. Generally, EC is usually used as a predominate solvent, where its

reduction product will be regarded as the main component of SEI. Lithium ethylene decarbonate ($(CH_2OCO2Li)_2$) is produced when the concentration of EC is high; in contrast, $LiCO_3$ will be produced with a low concentration of EC[2, 9-12]. The choice of graphite can supply good calendar life for commercial LIB. If the electrode material is Si, low Coulombic efficiency occurs due to its high capacity making SEI destroyed and unstable[6, 13, 14].

The quality of SEI affects the performance and cycle life of LIB[15]. The formation of SEI will be against further electrolyte decomposition since it prevents the transportation of electron. However, it still allows lithium ions through so that lithium could intercalate into the electrode to maintain long-term cycling life[1, 3, 7, 13, 16]. SEI forms due to the active lithium with its roughness and dendrites[13]. Therefore, an ideal SEI or a "good" SEI; it should be flexible and elastic with features: electronically insulating, maximum Li^+ conducting[1, 7, 13] and prevents unforeseen parasitic reactions[13]. Additionally, high resistance, high permeability of cations, and much thinner thickness about a few nanometers, these properties attribute to an ideal SEI as well[6].

SEI layer will form on the surface of active material AM (usually carbon compound), electrolyte can transport through the surface of AM to react with lithium and electrons[17], which leads to loss of AM. Zhang et al.[18] studied the mechanism of capacity fade, and there are two regimes; in their second regime, they concluded loss of AM is dominating. Besides, solvent reduction consumes lithium ions irreversibly. Losing active lithium is more severe, especially cycling life. Broussely et al.[19] show that the

consumption of lithium leads to aging performance. The final consequence is that irreversible capacity loss (ICL) induced by SEI[6, 7, 15] reduces LIB's calendar life. ICL usually occurs in the first cycle if the electrode is carbon[20]. Matsumura et al.[20] studied ICL by electrochemical methods and analytic techniques. They concluded that ICL not only on the decomposition of electrolyte but also on the status and amount of lithium. As depositing on the negative electrode at the lithiation process, the SEI layer prefers growing as a potential drop on the negative electrode[6]. Keil et al.[21] show that higher capacity loss and SEI growth can attribute to the lower potential of the negative electrode and high SOC. In Fig.5 in their literature, the potential reaches lowest at 60% SOC of NMC cell and 70% SOC of LFP cell; the corresponding capacity loss had also reached a large extent. As a passivation layer covering the surface of the negative electrode, SEI initially protects the electrode at the higher negative potential, but capacity fade occurs subsequently[3, 17, 22]. Other factors could modify SEI performance, such as kinetic reaction rate, species diffusion properties, temperature, etc. Thus, the SEI eventually becomes an essential factor to be considered upon the capacity fade in LIBs.

1.2 Open circuit voltage (OCV) storage

Self-discharge refers to the battery voltage drop that occurs spontaneously when the battery runs still under open-circuit conditions. There are two types of capacity loss[15]: reversible capacity loss (RCL) and ICL mentioned above. RCL can be recovered upon the charging process; however, ICL will not. So RCL will not be considered general in research and simulations. Johnson et al.[23] show that there is greater than 97% of initial capacity in 30 days under open circuit condition and conclude self-discharge is insignificant compared with the cycling life.

A charged LIB can self-discharge by coupling the solvent reduction reaction with a lithium deintercalation reaction without any driving force since there is no net current. The rate of self-discharge is limited by the rate of solvent reduction[15, 24]. Yazami et al.[25] presented a metastable electron-ion-electrolyte complex, which is formed and adsorbed on graphite during OCV storage. The complex is stable when the cell is charging after storage; it accounts for the capacity loss; the complex is unstable since absorbed electrons would transfer to an electrolyte. There is an irreversible reduction so that it accounts for ICL. ICL under OCV storage can be elaborated by the SEI layer growth covering the surface of the graphite electrode. There are no driving forces in our view, but the reactivity of lithium induces the deintercalation of lithium ions so that there is a range of potential where cause overpotential between SEI layer and electrode then driving force presents. The consumption of lithium to produce SEI, which causes lithium loss, also performs the SEI features mentioned above.

1.3 Mathematical modeling

The mathematical modeling method can make up the experiments' limitations especially thermodynamic and kinetics properties[13] and help understand battery science deeply; it can predict the range from electrons and the entire battery system[13]. As mentioned above, SEI may be harmless and cause ICL during storage; we might also regard solvent reduction reaction as the primary source of ICL and simulate the influence and growth of SEI when only the negative electrode is considered. The growth of SEI

might be controlled by diffusion of species and electrochemical kinetics; there will be various researchers done in the literature showing in chapter 2.

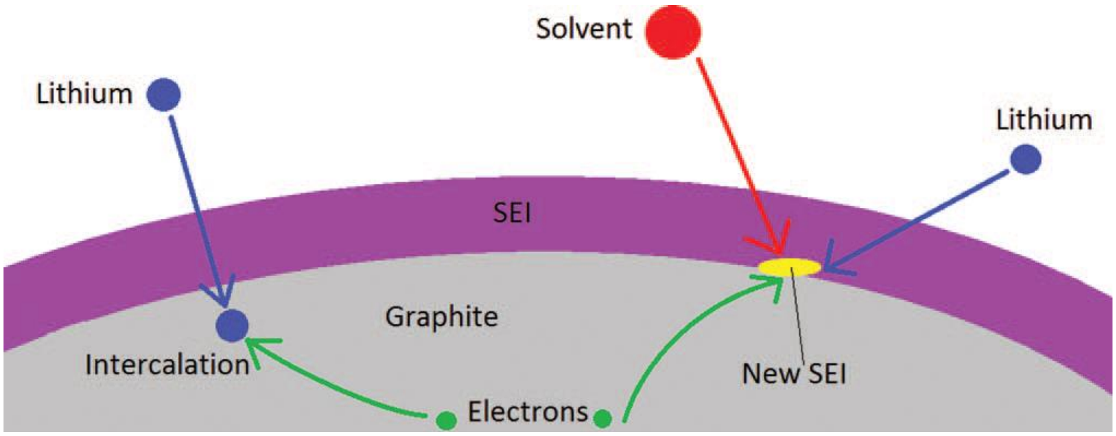

Figure 1.1 Schematic of SEI layer formation upon all elements[17]. Solvent molecules will react with lithium ions and electrons at the surface of electrode to form a new SEI layer.

CHAPTER 2

LITERATURE REVIEW

Capacity fade occurs during storage of lithium-ion battery cells. Several processes cause this capacity loss of lithium-ion batteries, including loss of active electrode material, loss of cyclable lithium ions and electrolyte decomposition due to parasitic electrochemical reactions on the electrode surface [26, 27]. The growth of solid electrolyte interface (SEI), which is a product from the parasitic reactions, inhibits further electrolyte decomposition[5]. In the literature, researchers have suggested that the growth of the SEI layer dominants the aging mechanism [17, 19, 28-55].

Zhang et al.[54] developed a single particle model to simulate the loss of lithium ions and listed various stages of capacity fade during the constant voltage storage, they calibrated against experimental data to obtain estimated parameters and proposed that the first stage of capacity loss is relevant with SEI. Ning et al.[40] developed a charge-discharge cycling model which regards solvent reduction reaction inducing loss of active lithium so that the process cause capacity fade. The exchange current density of parasitic reaction plays a role in capacity loss. Christensen et al.[29] and Colclasure et al.[30] utilize charged species transportation balance which dominates the growth of SEI to simulate in different coordinates; they listed many electrochemical reactions which are probably taking place in SEI and inducing growthof SEI with the corresponding kinetic

expressions, but they did not validate with the experimental data. The transportation of lithium ions in the layer also induces the formation of SEI[41, 51].

Based on the assumption that the diffusion of electrons through the SEI layer is rate-determining, the parabolic law models were developed by Peled et al.[5] and Broussely et al.[19], where the side reactions were assumed to occur on the interface between SEI layer and electrolyte. But Peled et al.[5] are not supported with any experimental data. Instead of assuming electron diffusion as rate-determining, Ploehn et al.[42]. proposed an SEI formation model by considering the solvent diffusion through the SEI porous layer as the rate-determining step, and the numerical results match with the experimental observations reasonably well. Yoshida et al.[53] tested the capacity fade and the thickness of SEI layer under 392 days storage upon the solvent diffusion assumption they built, and they proposed the aging of lithium ions batteries due to the growth of the SEI layer but they did not get a good agreement with experimental data of the thickness of SEI layer.

Sankarabramanian et al.[49] assumed the linear diffusion of the solvent through the SEI layer and used first order kinetics to describe side reactions; Deshpande et al.[32] extended Phul et al.[41] by adding the diffusion of the solvent but they did not get an agreement with the experimental data. Pinson et al.[17] used first-order kinetics and linear diffusion of solvent through SEI to express side reaction in the single-particle model by losing the lithium to show the formation of SEI on the negative electrode, and they applied Butler-Volmer kinetics and charged species conservation as an alternative way to describe the side reaction and simulated the SEI layer growth in the porous electrode model.

Lamorgese et al.[36], Ashwin et al.[28] ,Fu et al.[33] ,and Lin et al.[38] set up a pseudo-two-dimensional (P2D) model to simulate the SEI formation by applying porous electrode theory and the current density of side reaction which follows Tafel kinetics. Liu et al.[39] and Zhao et al.[55] added the solvent diffusion which follows Fick's second law through the SEI layer in their P2D simulation. Jin et al.[34] used a reduced-order approach to simplify the P2D model which contains solvent diffusion and Tafel kinetics, and they get good results with the experimental results. Kamyab et al.[35] extended Ploehn et al.'s[42] work by adding the Tafel kinetics within the film growth to mixed mode. They also assume the linear diffusion problem but with Tafel kinetics to solve an analytical solution of SEI film's thickness and capacity loss to compare with the experimental data under trickle charge storage. Rahamian et al[44] listed the kinetics-limited and diffusion-limited processes under extreme conditions to reveal that the growth of SEI is linear in the kinetic-limited region initially then the thickness is a function of the square root of time in the diffusion-limited region. Safari et al. [48] in 2008 proposed the diffusion of solvent and Tafel kinetics in a single-particle model under various conditions. They concluded that the growth of the film would be more controlled by diffusion; besides, under OCV storage, the values of the diffusion coefficient and reaction rate adjusted by them are relatively large. Safari et al.[47] in 2011 refined their equations and parameters to simulate their model again; they ignored the change of the open-circuit voltage and the influence of the initial SOC; after the improvement, they concluded that both diffusion and kinetics control the growth of the SEI film, and the growth of the film is maximized when the initial SOC is 100%.

The diffusion of a solvent through the film mixed with the electrochemical kinetics will describe the film growth. Ramasamy et al.[46] simulated zero-dimensional SEI growth and capacity loss under open-circuit conditions by using Tafel kinetics only; an ordinary differential equation is listed as to how lithium is consumed in the side reaction. In this work, we extend their model; by establishing a one-dimensional SEI film, the diffusion of the solvent in the film is added, which follows Fick's second law; electrochemistry reaction occurs at the interface between the SEI and the electrode. The reaction rate constant continues to follow, but the solvent concentration will be expressed as dependent variables in the exchange current density term. Besides, according to the theory of moving SEI film mentioned by Kamyab et al. [35] and Plohen et al.[42], the growth rate of SEI is obtained. The governing equations would predict the OCV value of electrode, SOC dropping, the SEI layer thickness, and the capacity loss. The OCV value prediction of the negative electrode is fitted to experimental data from a SONY 18650 lithium ions battery[56, 57]. Ramasamy et al.[46] plotted the OCV in their work. The effective diffusion coefficient of the solvent ($D_{s,eff}$) and the kinetic reaction rate of the SEI side reaction (k_{SEI}) are obtained from curve fitting to the experimental data. Additionally, we developed an alternative approach to solving nonlinear partial differential equation with Landau transformation. Making a moving boundary to be fixed, we can simulate the governing equations and boundary conditions in an easier sight and optimize the best-estimated parameters. The derivation process is shown in Appendix B.

CHAPTER 3

MODEL DEVELOPMENT

3.1 System geometry and physical assumptions

The solvent (S) and lithium ions (Li^{+}) diffuse through the SEI layer and react with the electrons on the electrode surface, which results in the formation of an insoluble product (P) at the electrode/SEI interface. The SEI growth on the electrode is shown schematically in Figure 3.1. In the present study, the model is developed to analyze the behavior of critical aging mechanisms and their impact on the capacity fade in the negative electrode. The following assumptions have been applied in the modeling of SEI growth under open circuit conditions.

1. Two components are in the system: porous domain of solvent (c_s) and lithium ions (Li^{+}) at the electrode surface.

2. We assume a porous structure for the SEI layer, the liquid electrolyte fills the pores of the SEI and reaches the electrode surface.

3. Diffusion of the solvent occurs only in the x direction; thus, the growth of the SEI is uniform in the y and z directions.

4. The overall self-discharge rate is so slow that it is not limited by diffusion of lithium ions out of the carbon electrode.

3.2 Electrochemical SEI reaction kinetics

The electrochemical reaction for SEI formation at the solid/electrolyte interface can be expressed as:

$$2Li^{+} + S + 2e^{-} \rightarrow P \tag{1}$$

A schematic of the electrode-SEI-electrolyte interface is shown in Figure 3.1. For an SEI layer much smaller in thickness than a typical particle of active material, the particle surface can be assumed to have zero curvature and is modeled in 1D cartesian coordinates. P represents the main inorganic component of solid electrolyte interphase (SEI). Christensen et al.[29]and Colclasure et al.[30] listed their reactions and utilized Li_2CO_3 as the main product. The releasing of flammable hydrocarbon methane gas is ignored in this work for simplicity. The rate of SEI formation reaction is affected by the mass transport of solvent and the kinetics. A Tafel expression is used to describe the kinetics of the irreversible formation reaction of the product (P) as:

$$J_{SEI} = -nFk_{SEI}c_s \frac{c_{Li^2}}{c_{Li,max}^2} \exp\left(-\frac{\alpha nF\eta_{SEI}}{RT}\right) \tag{2}$$

where k_{SEI} is the kinetic reaction rate constant and c_s is the solvent concentration in the SEI porous layer. The overpotential η_{SEI} is defined as

$$\eta_{SEI} = U^{OCP} - U_s^{SEI} \tag{3}$$

where U^{OCP} is the open-circuit potential of the anode, which is a function of SoC, as given in Appendix A; U_s^{SEI} is the irreversible open circuit potential for solvent reduction.

The solvent concentration is shown in the exchange current density term because the maximum solvent concentration is reduced; thus, solvent concentration to maximum solvent concentration disappears. Side reactions consume not only solvent but also active lithium. The consumption of lithium ions will be expressed by an ordinary differential equation since there is no net current. Therefore, the consumption of lithium is proportional to the current density of the side reaction.

$$\frac{1}{a}\frac{dc_{Li}}{dt} = \frac{J_{SEI}}{nF} \tag{4}$$

where a is a specific surface area whose value is listed in Table 3.1.

3.3 Solvent diffusion

Fick’s second law obtains a linear diffusion equation representing the solvent diffusion in the SEI layer in a moving boundary system.

$$\frac{\partial c_s}{\partial t} = D_s^{eff}\frac{\partial^2 c_s}{\partial x^2} \tag{5}$$

where c_s is the concentration of the solvent and D_s^{eff} is the effective diffusivity of the solvent.

$$D_s^{eff} = D_s \times \varepsilon_{SEI}^{1.5} \tag{6}$$

where D_s is the free stream diffusion coefficient of the solvent and ε_{SEI} is the SEI porosity. The above equation is valid in the region $x = 0$ to $x = L(t)$, where $L(t)$ represents the length of the SEI layer (SEI-electrode interface, see Figure 3.1).

The corresponding initial and boundary conditions are as follows. At the interface between the SEI and the electrolyte, the concentration is given by

$$c_s = \varepsilon_{SEI} c_{s,bulk} \text{ at } x = 0 \tag{7}$$

At the boundary between the SEI and the electrode, the solvent flux matches the side reaction current, which gives

$$-D_S^{eff} \frac{\partial c_s}{\partial x} = -\frac{J_{SEI}}{nF} \text{ at } x = L \tag{8}$$

where $c_{s,bulk}$ is the solvent concentration in the bulk of the electrolyte. Initially, the solvent concentration $c_s = \varepsilon_{SEI} c_{s,bulk}$ in the SEI layer.

3.4 Surface film thickness

SEI layers constitute the surface film covering the graphite electrode. In the model, the growth rate of SEI will be associated with the flux at the electrode/SEI interface, which is derived by Kamyab et al.[35]

$$\frac{dL}{dt} = -D_s^{eff} \frac{M_p}{\rho_p} \frac{dc_s}{dx}\bigg|_{x=L} \tag{9}$$

where M_p and ρ_p are molar weights and densities for the SEI layer. The ratio of the thickness to the molar weight corresponds to constant concentration for the SEI layer formed on negative electrodes, and they are given as c_p in Table 3.1.

3.5 Numerical solution technique

The mathematical model for the SEI growth under open-circuit conditions has two governing equations (Eqs. 5 and 6), which need to be solved simultaneously. These nonlinear partial differential equations are coupled with changing the thickness of the system due to the formation of the SEI (Eq. 10). This moving boundary problem can be transformed into a fixed boundary problem by introducing new space coordinates and applying the Landau transform. The transformations in the porous SEI medium $0 < x < L(t)$ is given by the following equation.

$$\xi = \frac{x}{L(t)} \tag{10}$$

where ξ is the dimensionless spatial positions in the SEI layer vary between 0 and 1. Applying this transformation results in a modification of the governing equations and boundary conditions. The change of coordinates and application of Landau transforms are described in Appendix B.

The modified equations were solved by using a commercial finite element package, COMSOL Multiphysics (version 5.6), and by using a fully implicit backward time centered space finite difference method in MATLAB. This converts the differential equations into nonlinear and linear equations, which were solved using MATLAB’s stiff

solver ode 15s. The OCP versus time curves from solutions for decreasing values of the grid spacing, h, is presented in Figure 3.2. The results from both the methods are consistent. All the simulations in this paper are performed on a PC with a 3.80 GHz processor and 64 GB RAM (running Windows 10).

3.6 Parameter estimation

To check the agreement of the mathematical model with the experimental data obtained on the SONY 18650 lithium-ion cell, the values of certain parameters in this model need to be estimated. Parameter estimation is a useful approach to find kinetic and transport parameters from the experimental data. Therefore, we used two methods in this work: the optimization module in COMSOL and a multi-parameter least square curve fitting procedure in MATLAB to interpret the data. Such techniques are typically formulated to minimize the sum-of-squared differences between the model outputs and their experimentally measured values.

$$\mathrm{Obj} = \min_{p} \left\{ \sum_{i=1}^{N} \left[\left(\mathrm{OCP}_i^{mod}\left(t_i, p\right) - \mathrm{OCP}_i^{exp}\left(t_i\right) \right)^2 \right] \right\} : \; p^l \le p \le p^u \qquad (11)$$

where subscripts mod and exp represent model and experimental results, and p^l, p^u are the lower and upper bounds for the parameters, respectively; N represents the number of time steps simulated. The nonlinear regression is performed using the Levenberg-Marquardt optimization algorithm in COMSOL Multiphysics and the least squares subroutine in MATLAB (LSQNONLIN). Therefore, by fitting the OCP curves, two parameters are estimated simultaneously with 95% confidence intervals: the kinetic reaction rate constant of side reaction and the effective diffusion coefficient of solvent.

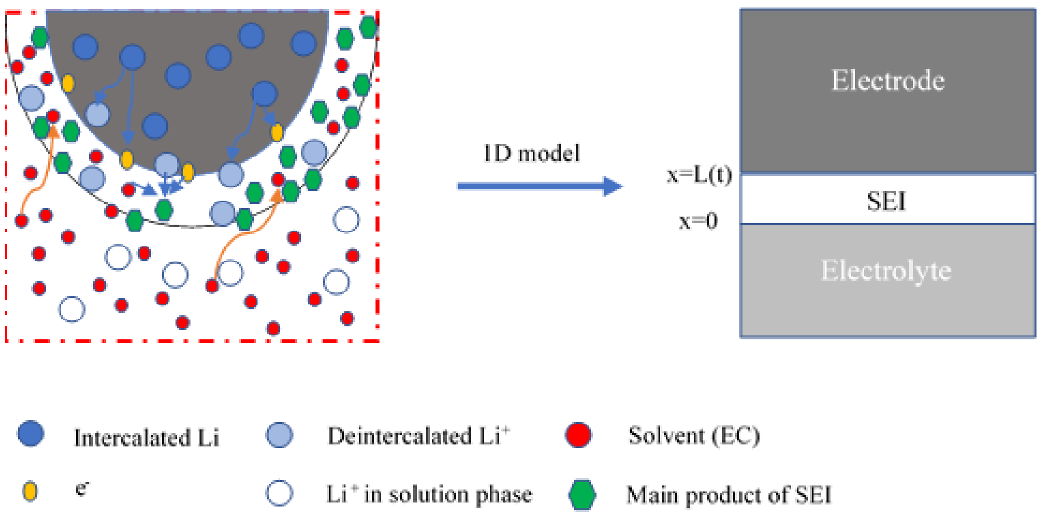

Figure 3.1. (a) Schematic illustration of the side reaction at the anode particle. (b) The right schematic is a one-dimensional SEI layer which is the projection from the particle.

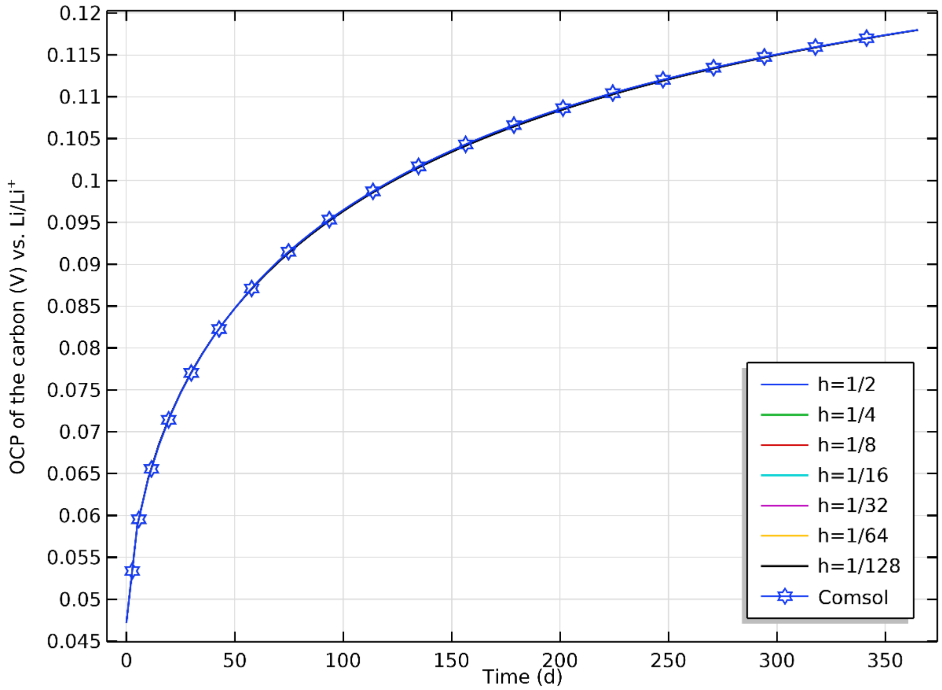

Figure 3.2. The OCP curves from solutions with different grid spacing h.

Table 3.1 Base-Case Values for Parameters used in the Modeling of SEI growth

Symbol (Unit)	Description	Value (ref)
Parameters of electrode and electrolyte		
$a(m^{-1})$	Specific surface area of the electrode	3×10^6[46]
$c_{Li,max}(mol/m^3)$	Maximum lithium concentration in the electrode	3.056×10^4[46]
$c_{s,bulk}(mol/m^3)$	Bulk solution of EC	4541[48]
Parameters of SEI layer		
$L_0(nm)$	Initial SEI film thickness	0.001*
$U_{SEI}(V)$	SEI formation equilibrium potential	0.4[35, 46]
ε_{SEI}	Porosity of SEI film	0.05[35, 48]
$c_p(mol/m^3)$	Constant concentration of SEI layer	28556[35]

* assumed

CHAPTER 4

RESULTS AND DISCUSSION

4.1 Connection of model with experiment

The OCV of the SONY 18650 lithium-ion cell as a function of time is reported in the literature by Ramasamy et al.[46]. Table 3.1 summarizes the design specifications and a list of characteristics of this cell. The OCP, SEI thickness, and capacity loss provide a better understanding of how different parameters such as D_s^{eff}, k_{SEI}, and ε_{SEI} are correlated with each other to obtain a certain OCP value and how a variation may affect the output.

The OCV vs. t data points for the SONY 18650 cell and the mixed mode model fit is shown in Figure 4.1. The kinetic limited model by Ramasamy et al.[46] is reproduced by assuming that the SEI growth occurs at the kinetic limited rate (i.e., the concentration of the solvent is present in excess at the anode/SEI film interface). Ramasamy et al.[46] assumed the SEI layer to be a non-porous solid phase and predicted that the capacity loss caused by the SEI growth changes linearly with the square root of time. As shown in Figure 4.1 here and in Figure 3 in Ref. 24, in which they fit their kinetic limited model predictions to their experimental data, it can be seen that the kinetic-limited model is only an approximate model. Also, the kinetic rate constant extracted from their fit is one order

of magnitude smaller $\left(1.5\times10^{-18}\ \mathrm{m/s}\right)$ than the kinetic rate constant in our mixed model. As shown in Figure 3.1, the overall quality of the mixed mode model predictions of the OCP data for the SONY 18650 cell demonstrates that the mixed mode model provides a satisfactory description of the OCP due to the growth of the SEI, which is valid for the entire time period that the lithium-ion cells were stored under open-circuit conditions.

The kinetic rate constant $\left(k_{SEI}\right)$ and the effective diffusion coefficient $\left(D_s^{eff}\right)$ extracted from the curve fitting to the experimental data points for the SONY 18650 cell, and the SEI parameters used in the model are listed in Tables 3.1 and 4.1. In addition, confidence intervals were obtained to provide an accuracy range for the estimated parameters. As the values in Table 4.1 indicate, the kinetics and effective diffusion parameters based on the two numerical approaches (finite element and finite difference methods) are reasonably close to each other, demonstrating the credibility of the mixed mode model to simulate the growth of the SEI layer. Diffusion coefficients are calculated according to Eq. 6 without any confidence intervals are listed in Table 4.1.

4.2 Diffusion coefficient and kinetic rate constant parametric study

The chemical kinetics and transport properties of the SEI growth model, such as the kinetic rate constant of the solvent reduction reaction and diffusion coefficient of the solvent, are critical in estimating open circuit potential, SEI thickness, and capacity loss. To investigate the effect of the diffusion coefficient of the solvent, OCP predictions for different diffusion coefficient values are shown in Figure 4.2 for the SONY 18650 cell. As shown in Figure 4.2, the higher diffusion coefficient of the solvent results in a higher

OCP value due to faster diffusion of the solvent. In other words, the film growth rate at the negative electrode is greater for the higher diffusion coefficients.

A similar parametric study was conducted to evaluate the effect of the kinetic rate constant of the solvent reduction reaction on the OCP and OCP predictions for different k_{SEI} values are shown in Figure 4.3 for the SONY 18650 cell. The solid curves fitted to the measurement data points are the simulation result for $k_{SEI} = 1.6434 \times 10^{-17}$ m/s . As Figure 4.3 illustrates, OCP value increases more rapidly with time for higher k_{SEI} value due to a higher rate of SEI formation. The dependency of the OCP on the kinetic rate constant of the solvent reduction reaction can be explained through the correlation between the Tafel kinetics and the growth rate of the SEI layer shown in Eqs. 2 and 9.

4.3 Solvent concentration

The current model equations have been evaluated for concentration profiles in the SEI layer for 365 days. Figure 4.4 shows the plots for the variation of concentration with time at the electrode/SEI interface of the SONY 18650 cell. Initially, solvent consumption is expected to be higher, manifested in the faster rate of SEI formation or the moving boundary velocity. Under these circumstances, the diffusion of solvent ions reaches a steady state, and the SEI layer grows faster and thicker. As the time increases, the concentration profile drops and rises as the interface shifts towards higher solvent concentrations. The drop in concentration occurs as the Li^{+} ions at the interface are depleted. The rise occurs as the diffusion occurs, increasing the solvent concentration at the interface as it moves.

4.4 SEI thickness

It is important to understand the relationship among diffusivity, side reaction rate, and SEI layer growth characteristics. When the diffusion coefficient is small, the system becomes diffusion limited. Figure 4.5 shows the SEI layer growth with different diffusion coefficients for the solvent in the SEI layer. On the other hand, with a large diffusion coefficient, the system becomes more kinetics limited. For example, with the diffusion coefficients varied by two orders of magnitude, the SEI layer grows two times thick. This is because the solvent diffuses through the porous SEI layer more easily to reach the electrode surface with a higher diffusion coefficient. Therefore, the SEI layer grows faster and thicker.

The SEI layer growth also depends on the kinetics of the side reaction. Figure 4.6 shows the effect of the side reaction rate constant on SEI growth. The reaction rate is varied by two orders of magnitude. The SEI layer grows faster and thicker with a faster reaction rate. The overall trend is that the SEI layer grows quickly initially. This is because the initial growth of SEI is diffusion limited. Then, the growth rate gradually slows down due to the rising resistance from the layer thickness, making the system shift toward kinetic limited.

Ramasamy et al. [46] derived their expression for the SEI thickness using a kinetic limited model that increases continuously over time due to the solvent reduction reaction (see Eq. 13 in Ref. 24). In addition, they assumed the solvent is present in excess at the electrode/SEI film interface and thus do not limit the reduction reaction rate and the rate constant for the side reaction, k_{SEI} to be 1.5×10^{-18} m/s (see Figure 3 caption in Ref. 24).

Figure 4.7 shows their model prediction for the SEI thickness, which greatly deviates (almost 1.5 times more) from our mixed mode model prediction.

4.5 Capacity loss

The capacity loss is proportional to the current density of the side reaction. Therefore, the loss of active lithium-ions per unit surface area during storage was estimated using the following equation:

$$\text{Capacity loss} = \int_0^{t_{final}} \left| J_{SEI} \right| dt \tag{12}$$

Figure 4.8 shows the capacity loss due to SEI growth from our mixed-mode model and comparison with Ramasamy et al.'s[46] kinetic limited model that increases continuously over time due to the solvent reduction reaction (see Eq. 10 in Ref. 24). Their model prediction for the capacity loss greatly deviates (almost 1.5 times more)

Table 4.1 Model parameters for the 1D cell simulation model

Parameters	**COMSOL**	**MATLAB**
$k_{SEI}\left(m/s\right)$	$1.6434\times10^{-17}\pm4.3424\times10^{-18}$	$1.6545\times10^{-17}\pm4.6825\times10^{-18}$
$D_s^{eff}\left(m^2/s\right)$	$1.4029\times10^{-19}\pm4.3755\times10^{-20}$	$1.4213\times10^{-19}\pm4.7289\times10^{-20}$
$D_s\left(m^2/s\right)=D_s^{eff}\times\varepsilon_{SEI}^{-1.5}$	1.2548×10^{-17}	1.2712×10^{-17}

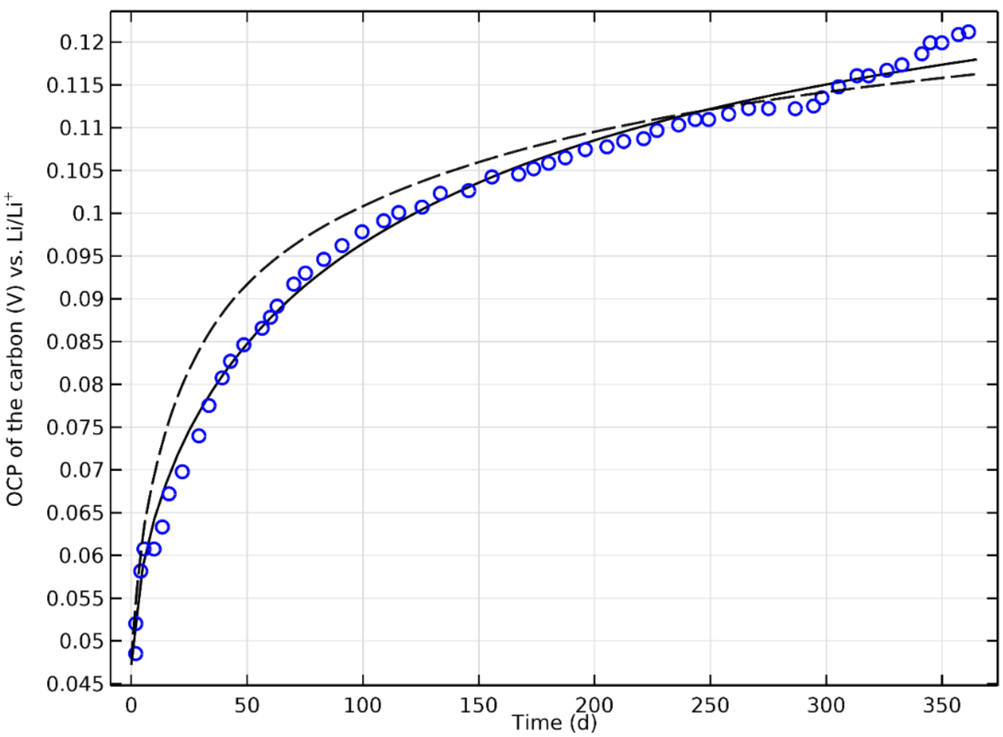

Figure 4.1 Data for the SONY 18650 cell stored at 100% SOC over 365 days (o). The lines are from the numerical solution of our mixed mode model (—) and kinetic limited model [46] (- - -) for OCP of negative electrode as a function of time in days.

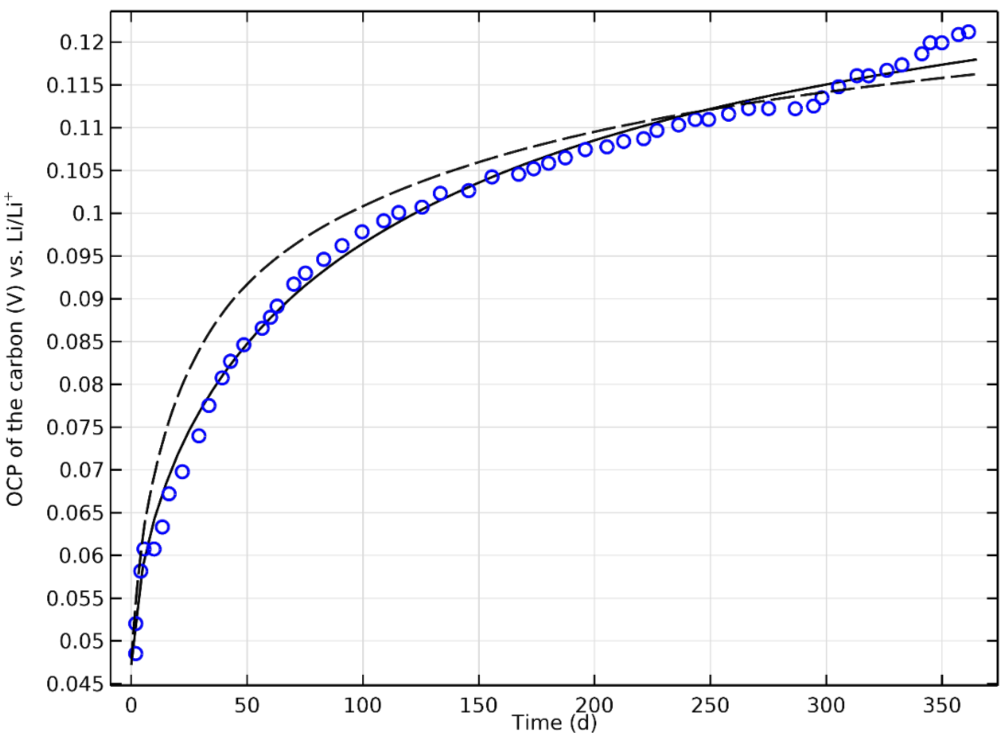

Figure 4.2 Measured (O) and simulated (—) capacity loss as function of time for different diffusion coefficient D_s^{eff} Values.

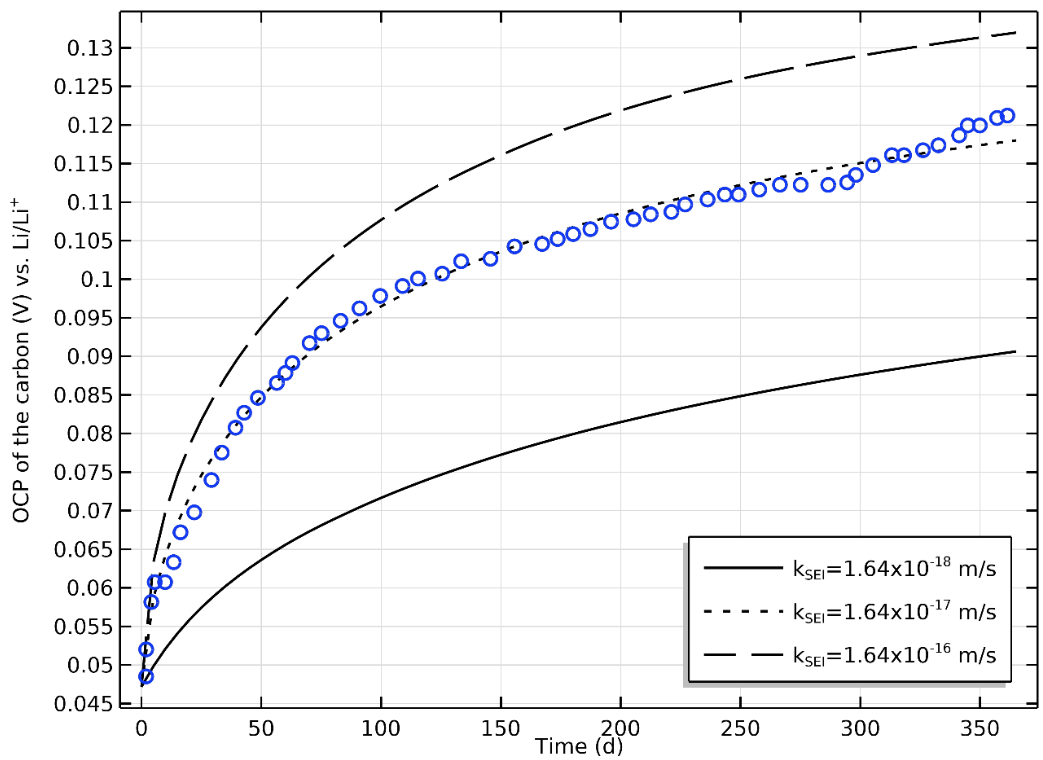

Figure 4.3 Measured (O) and simulated (—) capacity loss as function of time for different reaction rate constant k_{SEI} Values.

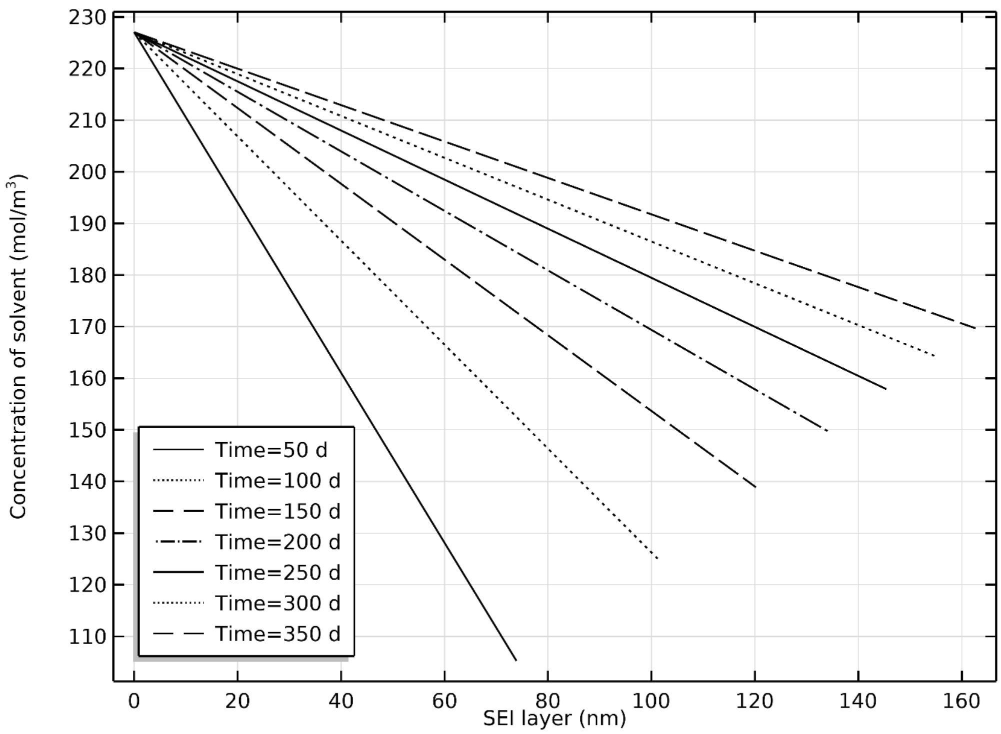

Figure 4.4 Solvent concentration versus SEI thickness in mixed mode model over 365 days.

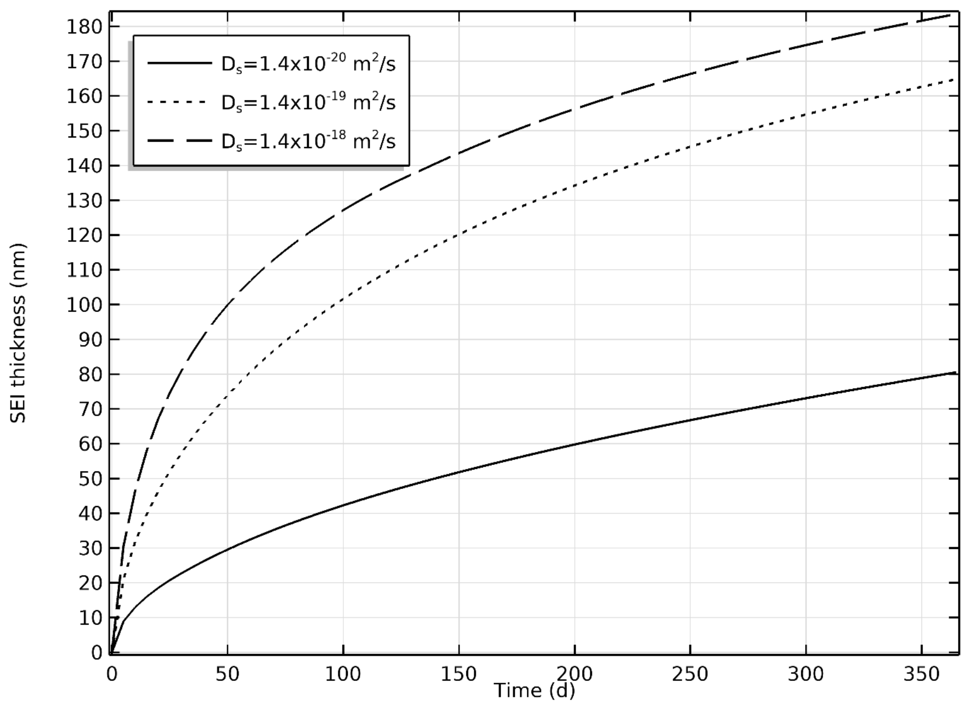

Figure 4.5 Effect of solvent diffusion coefficient on SEI growth.

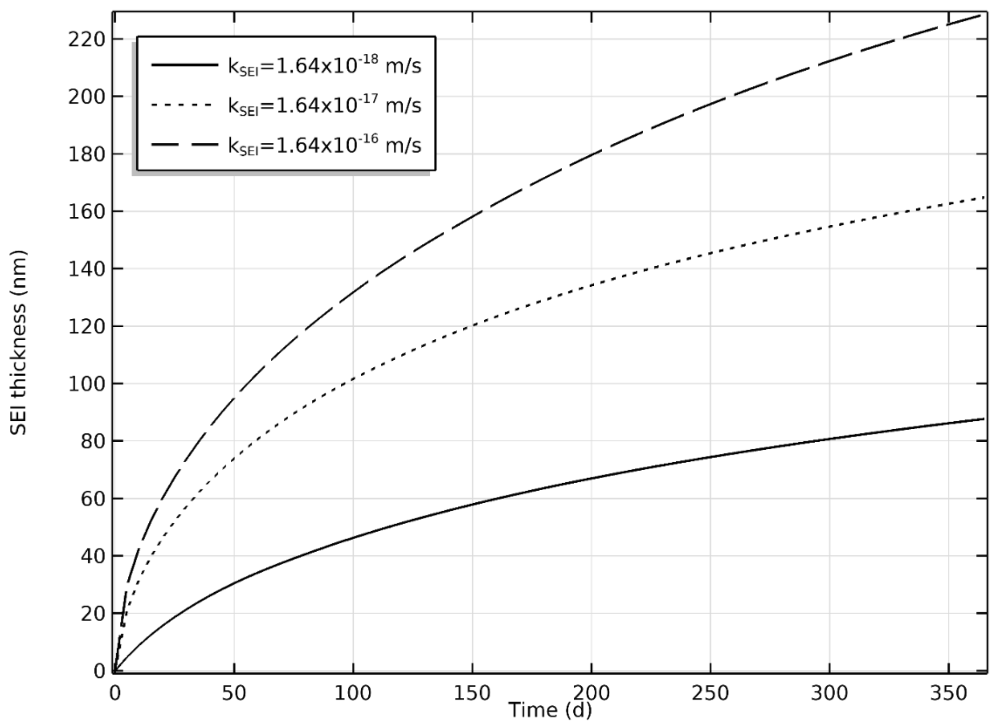

Figure 4.6 Effect of kinetic reaction rate constant on SEI growth. Higher reaction rate causing thicker SEI thickness.

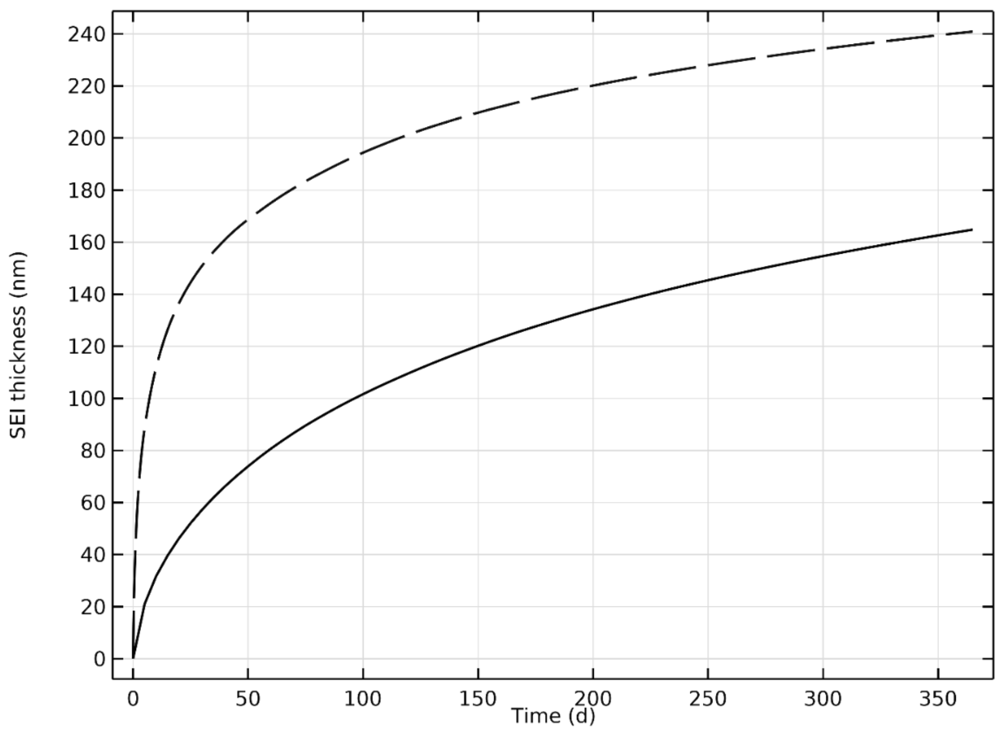

Figure 4.7 SEI thickness as a function of time in our mixed mode model (—) and reproduced solutions from reference Ramasamy et al. [46] (- -). Ramasamy et al.'s Eq.13 with the rate constant of $k_{SEI} = 1.5 \times 10^{-18}\ m/s$ greatly deviates from our model.

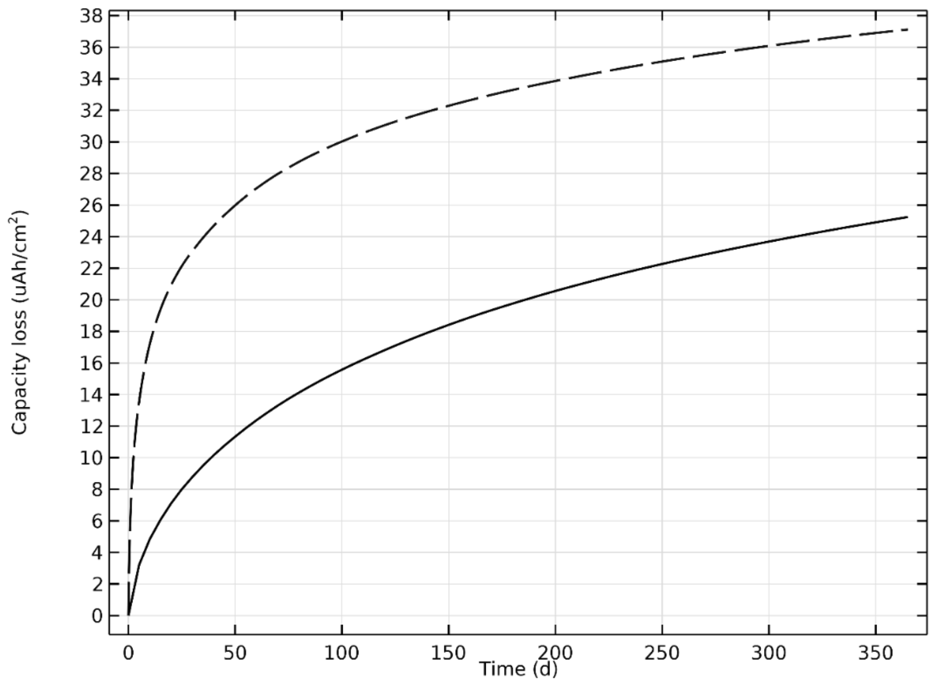

Figure 4.8 Capacity loss as a function of time in our mixed mode model (—) and reproduced solutions from reference Ramasamy et al. [46] (- -). Ramasamy et al.'s Eq.10 with the rate constant of $k_{SEI} = 1.5 \times 10^{-18}$ m/s greatly deviates from our model.

CHAPTER 5

CONCLUSION

5.1 Summary

In this study, the SEI layer growth was modeled as a side reaction of solvent reduction at the anode under open-circuit conditions. The SEI layer grows depending on the diffusion of solvent through SEI layer and its corresponding reaction Tafel kinetics with the deintercalated lithium ions where it is associated with current density of side reaction at the electrode/SEI interface. The experimental data for OCV storage from the literature is fitted and results present the mixed mode simulation displaying less capacity loss and thinner SEI thickness due to the growth of the SEI film under open circuit condition than previous results presented by others[46]. In the OCV storage process, lithium ions will de-intercalate from the negative electrode, then the decreasing of the SOC induces the rise of OCV value of the negative electrode. The different magnitude of effective diffusion coefficient of solvent and side reaction rate both play roles in affecting SEI growth. An alternative approach, for solving partial differential equations, which fixes moving boundary problem, is computed by COMSOL and MATLAB to get accurate estimated parameters and confidence intervals. These two methods are finite elements method and finite difference method, the result are consistent so that it is convinced to simulate. The estimated parameters using in this work are validated with the experimental data in literatures.

5.2 Future work

There is a self-discharge process under 1D SEI model with Fick's law, Tafel kinetics which is shown in this thesis. Works of literature show that SEI layer growth and other properties under various conditions. The simulation aims to keep the lifetime of batteries to avoid external and internal factors. However, we did not contain the influence of temperature. In future work, we should add the temperature conservation in the SEI layer and the Arrhenius equations to describe how temperature affects the diffusion coefficient of solvent the side reaction rate constant[44, 55]. There will be another essential work to research on various storage for the battery for lessening the capacity loss in the future.

REFERENCES

1. Cheng, X.B., et al., *A review of solid electrolyte interphases on lithium metal anode.* Advanced science, 2016. **3**(3): p. 1500213.
2. Aurbach, D., et al., *The correlation between the surface chemistry and the performance of Li-carbon intercalation anodes for rechargeable 'Rocking-Chair'type batteries.* Journal of The Electrochemical Society, 1994. **141**(3): p. 603.
3. Heiskanen, S.K., J. Kim, and B.L. Lucht, *Generation and evolution of the solid electrolyte interphase of lithium-ion batteries.* Joule, 2019. **3**(10): p. 2322-2333.
4. Xu, K., *Nonaqueous liquid electrolytes for lithium-based rechargeable batteries.* Chemical reviews, 2004. **104**(10): p. 4303-4418.
5. Peled, E., *The electrochemical behavior of alkali and alkaline earth metals in nonaqueous battery systems—the solid electrolyte interphase model.* Journal of The Electrochemical Society, 1979. **126**(12): p. 2047.
6. Peled, E. and S. Menkin, *SEI: past, present and future.* Journal of The Electrochemical Society, 2017. **164**(7): p. A1703.
7. Verma, P., P. Maire, and P. Novák, *A review of the features and analyses of the solid electrolyte interphase in Li-ion batteries.* Electrochimica Acta, 2010. **55**(22): p. 6332-6341.
8. Yang, C., Y. Wang, and C. Wan, *Composition analysis of the passive film on the carbon electrode of a lithium-ion battery with an EC-based electrolyte.* Journal of power sources, 1998. **72**(1): p. 66-70.
9. Aurbach, D., et al., *Failure and stabilization mechanisms of graphite electrodes.* The Journal of Physical Chemistry B, 1997. **101**(12): p. 2195-2206.
10. Aurbach, D., et al., *The study of surface film formation on noble-metal electrodes in alkyl carbonates/Li salt solutions, using simultaneous in situ AFM, EQCM, FTIR, and EIS.* Langmuir, 1999. **15**(8): p. 2947-2960.

11. Li, T. and P.B. Balbuena, *Theoretical studies of the reduction of ethylene carbonate.* Chemical Physics Letters, 2000. **317**(3-5): p. 421-429.
12. Wang, Y., et al., *Theoretical studies to understand surface chemistry on carbon anodes for lithium-ion batteries: reduction mechanisms of ethylene carbonate.* Journal of the American Chemical Society, 2001. **123**(47): p. 11708-11718.
13. Wang, A., et al., *Review on modeling of the anode solid electrolyte interphase (SEI) for lithium-ion batteries.* Computational Materials, 2018. **4**(1): p. 1-26.
14. Zhang, W.-J., *A review of the electrochemical performance of alloy anodes for lithium-ion batteries.* Journal of Power Sources, 2011. **196**(1): p. 13-24.
15. Arora, P., R.E. White, and M. Doyle, *Capacity fade mechanisms and side reactions in lithium-ion batteries.* Journal of the Electrochemical Society, 1998. **145**(10): p. 3647.
16. Fong, R., U. Von Sacken, and J.R. Dahn, *Studies of lithium intercalation into carbons using nonaqueous electrochemical cells.* Journal of The Electrochemical Society, 1990. **137**(7): p. 2009.
17. Pinson, M.B. and M.Z. Bazant, *Theory of SEI formation in rechargeable batteries: capacity fade, accelerated aging and lifetime prediction.* Journal of the Electrochemical Society, 2012. **160**(2): p. A243.
18. Zhang, Q. and R.E. White, *Calendar life study of Li-ion pouch cells.* Journal of Power Sources, 2007. **173**(2): p. 990-997.
19. Broussely, M., et al., *Aging mechanism in Li ion cells and calendar life predictions.* Journal of Power Sources, 2001. **97**: p. 13-21.
20. Matsumura, Y., S. Wang, and J. Mondori, *Mechanism leading to irreversible capacity loss in Li ion rechargeable batteries.* Journal of the Electrochemical Society, 1995. **142**(9): p. 2914.
21. Keil, P., et al., *Calendar aging of lithium-ion batteries.* Journal of The Electrochemical Society, 2016. **163**(9): p. A1872.
22. Attia, P.M., et al., *Electrochemical kinetics of SEI growth on carbon black: part I. Experiments.* Journal of The Electrochemical Society, 2019. **166**(4): p. E97.
23. Johnson, B.A. and R.E. White, *Characterization of commercially available lithium-ion batteries.* Journal of power sources, 1998. **70**(1): p. 48-54.

24. Wang, C., et al., *Self-discharge of secondary lithium-ion graphite anodes.* Journal of Power Sources, 2002. **112**(1): p. 98-104.

25. Yazami, R. and Y.F. Reynier, *Mechanism of self-discharge in graphite–lithium anode.* Electrochimica Acta, 2002. **47**(8): p. 1217-1223.

26. Aurbach, D., et al., *The study of electrolyte solutions based on ethylene and diethyl carbonates for rechargeable Li batteries: II. Graphite electrodes.* Journal of The Electrochemical Society, 1995. **142**(9): p. 2882.

27. Jang, D.H., Y.J. Shin, and S.M. Oh, *Dissolution of spinel oxides and capacity losses in 4 V li/li x Mn2 O 4 cells.* Journal of the Electrochemical Society, 1996. **143**(7): p. 2204.

28. Ashwin, T., et al., *Modified electrochemical parameter estimation of NCR18650BD battery using implicit finite volume method.* Journal of Power Sources, 2017. **341**: p. 387-395.

29. Christensen, J. and J. Newman, *A mathematical model for the lithium-ion negative electrode solid electrolyte interphase.* Journal of The Electrochemical Society, 2004. **151**(11): p. A1977.

30. Colclasure, A.M., K.A. Smith, and R.J. Kee, *Modeling detailed chemistry and transport for solid-electrolyte-interface (SEI) films in Li–ion batteries.* Electrochimica Acta, 2011. **58**: p. 33-43.

31. Delacourt, C. and M. Safari, *Life simulation of a graphite/LiFePO4 cell under cycling and storage.* Journal of The Electrochemical Society, 2012. **159**(8): p. A1283.

32. Deshpande, A., S. Phul, and B. Krishnamurthy, *A generalized mathematical model to understand the capacity fading in lithium ion batteries-Effects of solvent and lithium transport.* Journal of Electrochemical Science and Engineering, 2015. **5**(3): p. 181-195.

33. Fu, R., et al., *Development of a physics-based degradation model for lithium ion polymer batteries considering side reactions.* Journal of Power Sources, 2015. **278**: p. 506-521.

34. Jin, X., et al., *Physically-based reduced-order capacity loss model for graphite anodes in Li-ion battery cells.* Journal of Power Sources, 2017. **342**: p. 750-761.

35. Kamyab, N., J.W. Weidner, and R.E. White, *Mixed mode growth model for the solid electrolyte interface (SEI).* Journal of The Electrochemical Society, 2019. **166**(2): p. A334.
36. Lamorgese, A., R. Mauri, and B. Tellini, *Electrochemical-thermal P2D aging model of a LiCoO2/graphite cell: Capacity fade simulations.* Journal of Energy Storage, 2018. **20**: p. 289-297.
37. Lee, J.-W., Y.K. Anguchamy, and B.N. Popov, *Simulation of charge–discharge cycling of lithium-ion batteries under low-earth-orbit conditions.* Journal of Power Sources, 2006. **162**(2): p. 1395-1400.
38. Lin, X., et al., *A comprehensive capacity fade model and analysis for Li-ion batteries.* Journal of The Electrochemical Society, 2013. **160**(10): p. A1701.
39. Liu, L., et al., *A thermal-electrochemical model that gives spatial-dependent growth of solid electrolyte interphase in a Li-ion battery.* Journal of power sources, 2014. **268**: p. 482-490.
40. Ning, G. and B.N. Popov, *Cycle life modeling of lithium-ion batteries.* Journal of The Electrochemical Society, 2004. **151**(10): p. A1584.
41. Phul, S., A. Deshpande, and B. Krishnamurthy, *A Mathematical model to study the effect of potential drop across the SEI layer on the capacity fading of a lithium ion battery.* Electrochimica Acta, 2015. **164**: p. 281-287.
42. Ploehn, H.J., P. Ramadass, and R.E. White, *Solvent diffusion model for aging of lithium-ion battery cells.* Journal of The Electrochemical Society, 2004. **151**(3): p. A456.
43. Prasad, G.K. and C.D. Rahn, *Model based identification of aging parameters in lithium ion batteries.* Journal of power sources, 2013. **232**: p. 79-85.
44. Rahimian, S.K., et al., *A generalized physics-based calendar life model for Li-ion cells.* Electrochimica Acta, 2020. **348**: p. 136343.
45. Ramadass, P., et al., *Development of first principles capacity fade model for Li-ion cells.* Journal of the Electrochemical Society, 2004. **151**(2): p. A196.
46. Ramasamy, R.P., J.-W. Lee, and B.N. Popov, *Simulation of capacity loss in carbon electrode for lithium-ion cells during storage.* Journal of power sources, 2007. **166**(1): p. 266-272.

47. Safari, M. and C. Delacourt, *Simulation-based analysis of aging phenomena in a commercial graphite/LiFePO4 cell.* Journal of The Electrochemical Society, 2011. **158**(12): p. A1436.
48. Safari, M., et al., *Multimodal physics-based aging model for life prediction of Li-ion batteries.* Journal of The Electrochemical Society, 2008. **156**(3): p. A145.
49. Sankarasubramanian, S. and B. Krishnamurthy, *A capacity fade model for lithium-ion batteries including diffusion and kinetics.* Electrochimica Acta, 2012. **70**: p. 248-254.
50. Santhanagopalan, S., et al., *Review of models for predicting the cycling performance of lithium ion batteries.* Journal of power sources, 2006. **156**(2): p. 620-628.
51. Shi, S., et al., *Direct calculation of Li-ion transport in the solid electrolyte interphase.* Journal of the American Chemical Society, 2012. **134**(37): p. 15476-15487.
52. Yang, X.-G., et al., *Modeling of lithium plating induced aging of lithium-ion batteries: Transition from linear to nonlinear aging.* Journal of Power Sources, 2017. **360**: p. 28-40.
53. Yoshida, T., et al., *Degradation mechanism and life prediction of lithium-ion batteries.* Journal of The Electrochemical Society, 2006. **153**(3): p. A576.
54. Zhang, Q. and R.E. White, *Capacity fade analysis of a lithium ion cell.* Journal of Power Sources, 2008. **179**(2): p. 793-798.
55. Zhao, Y., S.-Y. Choe, and J. Kee, *Modeling of degradation effects and its integration into electrochemical reduced order model for Li (MnNiCo) O2/Graphite polymer battery for real time applications.* Electrochimica Acta, 2018. **270**: p. 440-452.
56. Ramasamy, R.P., et al., *Synthesis, characterization and cycling performance of novel chromium oxide cathode materials for lithium batteries.* Journal of power sources, 2003. **124**(1): p. 155-162.
57. Ramasamy, R.P., R.E. White, and B.N. Popov, *Calendar life performance of pouch lithium-ion cells.* Journal of Power Sources, 2005. **141**(2): p. 298-306.

APPENDIX A

OPEN-CIRCUIT FUNCTION

The OCV of carbon electrode is a function of SOC[35, 45, 46, 48]:

$$U_{eq} = \begin{pmatrix} 0.7222 + 0.1387\mathrm{SoC} + 0.029\mathrm{SoC}^{0.5} - 0.0172\mathrm{SoC}^{-1} + 0.0019\mathrm{SoC}^{-1.5} \\ +0.2802\exp\left(0.9 - 15\mathrm{SoC}\right) - 0.7984\exp\left(0.4465\mathrm{SoC} - 0.4108\right) \end{pmatrix}(\mathrm{V}) \qquad [\mathrm{A1}]$$

APPENDIX B

CHANGE OF COORDINATES AND APPLICATION OF LANDAU TRANSFORMS

The moving boundary problem can be converted into a fixed boundary problem by introducing new spatial coordinates in dimensionless form through the application of Landau transforms. Consider f as a variable to replace c_s, which is a function of spatial direction (x) and time (t), and L is a function of time (t). By transforming the original system of equations into a new system, based on Eqs.5 and 10, f becomes a function of time (t) and the dimensionless spatial variable (ξ).

According to the chain rule, the derivatives of f in the original, moving boundary (mov) coordinates, and new, fixed boundary (fix) coordinates are related as

$$\left(\frac{\partial f}{\partial t}\right)_{mov} = \left(\frac{\partial f}{\partial t}\right)_{fix} \frac{\partial t}{\partial t} + \left(\frac{\partial f}{\partial \xi}\right)_{fix} \frac{\partial \xi}{\partial t} = \left(\frac{\partial f}{\partial t}\right)_{fix} + \left(\frac{\partial f}{\partial \xi}\right)_{fix} \frac{\partial \xi}{\partial t} \quad \text{[B1]}$$

$$\left(\frac{\partial f}{\partial x}\right)_{mov} = \left(\frac{\partial f}{\partial t}\right)_{fix} \frac{\partial t}{\partial x} + \left(\frac{\partial f}{\partial \xi}\right)_{fix} \frac{\partial \xi}{\partial x} = \left(\frac{\partial f}{\partial \xi}\right)_{fix} \frac{\partial \xi}{\partial x} \quad \text{[B2]}$$

$$\left(\frac{\partial^2 f}{\partial x^2}\right)_{mov} = \left(\frac{\partial^2 f}{\partial \xi^2}\right)_{fix}^2 \left(\frac{\partial \xi}{\partial x}\right)^2 \quad \text{[B3]}$$

Substituting the derivatives of the dimensionless spatial position ξ into the governing equations in the SEI layer, we have

$$\left(\frac{\partial f}{\partial t}\right)_{mov} = \left(\frac{\partial f}{\partial t}\right)_{fix} - \frac{\xi}{L}\frac{\partial L}{\partial t}\left(\frac{\partial f}{\partial \xi}\right)_{fix} \quad [B4]$$

$$\left(\frac{\partial f}{\partial x}\right)_{mov} = \frac{1}{L}\left(\frac{\partial f}{\partial \xi}\right)_{fix} \quad [B5]$$

$$\left(\frac{\partial^2 f}{\partial x^2}\right)_{mov} = \frac{1}{L^2}\left(\frac{\partial^2 f}{\partial \xi^2}\right)_{fix} \quad [B6]$$

Therefore, by applying the Landau transformation (Eqs. B4 to B6), the governing Eq. 5 is transformed to

$$\frac{\partial c_s}{\partial t} = \frac{D_s^{eff}}{L^2}\frac{\partial^2 c_s}{\partial \xi^2} + \frac{\xi}{L}\frac{\partial L}{\partial t}\frac{\partial c_s}{\partial \xi} \quad [B7]$$

Further, the velocity of the moving interface is expressed as

$$\frac{\partial L}{\partial t} = -D_s^{eff}\frac{M_p}{\rho_p}\frac{1}{L}\left.\frac{\partial c_s}{\partial \xi}\right|_{\xi=1} \quad [B8]$$

The boundary conditions for Eq. B7 are transformed to

$$c_s = \varepsilon_{SEI} c_{s,bulk} \text{ at } \xi = 0 \quad [B9a]$$

$$-D_s^{eff}\frac{1}{L}\frac{\partial c_s}{\partial \xi} = -\frac{J_{SEI}}{nF} \text{ at } \xi = 1 \quad [B9b]$$

The partial differential equations (PDEs) for concentration and velocity within the porous SEI layer obtained after Landau transformation, Eqs. B7 and B8, were discretized using finite difference method. Eqs. B10 and B11 show the discretized form for the transformed PDEs.

$$\frac{\partial c_{s,i}}{\partial t} = \frac{D_s^{eff}}{L^2}\frac{\left(c_{s,i-1} - 2c_{s,i} + c_{s,i+1}\right)}{h^2} + \frac{1}{2}\frac{\partial L}{\partial t}\frac{ih}{L}\frac{\left(c_{s,i-1} - c_{s,i+1}\right)}{h} \qquad [B10]$$

$$\frac{\partial L}{\partial t} = -D_s^{eff}\frac{M_p}{\rho_p}\frac{1}{L}\left.\frac{\left(c_{s,N-1} - 4c_{s,N} + 3c_{s,N+1}\right)}{2h}\right|_{\xi=1} \qquad [B11]$$

where i ranges from 1 to $N = 101$. The discretized boundary conditions for c_s are also written below.

$$c_s = \varepsilon_{SEI} c_{s,bulk} \text{ at } \xi = 0 \qquad [B12a]$$

$$-D_s^{eff}\frac{1}{L}\frac{\left(c_{s,N-1} - 4c_{s,N} + 3c_{s,N+1}\right)}{2h} = -\frac{J_{SEI}}{nF} \text{ at } \xi = 1 \qquad [B12b]$$

APPENDIX C

COMPUTATION IN COMSOL

The governing equations are transformed as an alternative form by using Landau transformation where is shown in Appendix B. The equations are solved in commercial finite elements package, COMSOL Multiphysics, and by using a finite difference method in MATLAB.

Finite elements are numerically solved by COMSOL, and its brief report is shown. Because we use the dimensionless independent variable, all parameters are also without their units to compute.

1 Global Definitions

1.1 PARAMETERS

PARAMETERS 1

Name	Expression	Value	Description
Ceq	4541	4541	
cp	28556	28556	
Ds0	1.2e-19	1.2E−19	
L0	1e-12	1E−12	
k0_SEI0	6e-17	6E−17	
F	96485	96485	
U_SEI	0.4	0.4	
R	8.3145	8.3145	
T	298.15	298.15	
epsilonSEI	0.05	0.05	
n	2	2	
a	3e6	3E6	
cLimax	3.056e4	30560	
xi	1	1	
kp	1	1	

2 Component 1

SETTINGS

Description	Value
Unit system	Same as global system

2.1 DEFINITIONS

2.1.1 Variables

Variables 1

SELECTION

Geometric entity level	Entire model

Name	Expression	Unit	Description
J_SEI	-i0*(soc_N)^2*exp(-0.5*F*eta_SEI*n/R/T)		
i0	n*F*k0_SEI*cs		
soc_N	cLi/cLimax		
eta_SEI	U - U_SEI		
U	Un(soc_N)		
Ds	Ds0		
k0_SEI	k0_SEI0		

2.1.2 Functions

Analytic 1

Function name	Un
Function type	Analytic

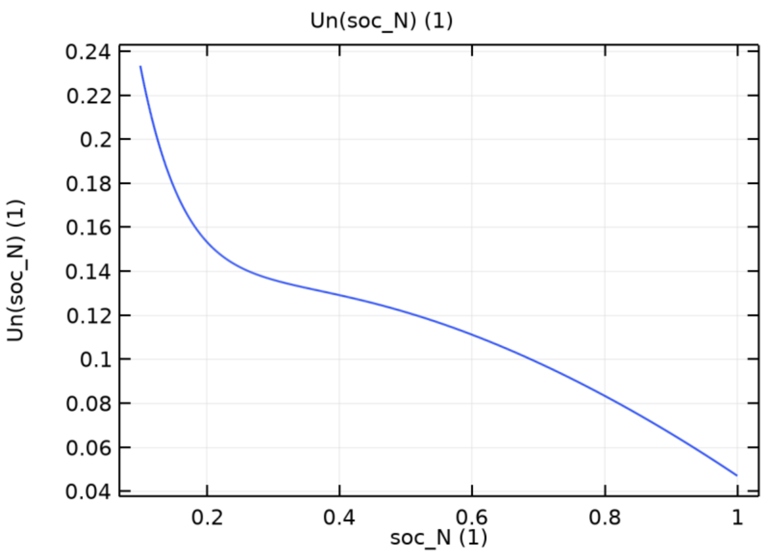

Analytic 1

DEFINITION

Description	Value
Expression	0.7222 + 0.1387*soc_N + 0.029*soc_N^(1/2) -0.0172/soc_N + 0.0019/soc_N^1.5 + 0.2802*exp(0.9 - 15*soc_N) - 0.7984*exp(0.4465*soc_N - 0.4108)
Arguments	soc_N

UNITS

Description	Value
Arguments	1
Function	1

2.1.3 Nonlocal Couplings

Integration 1

Coupling type	Integration
Operator name	intop1

SELECTION

Geometric entity level	Boundary
Selection	Geometry geom1: Dimension 0: Boundary 1

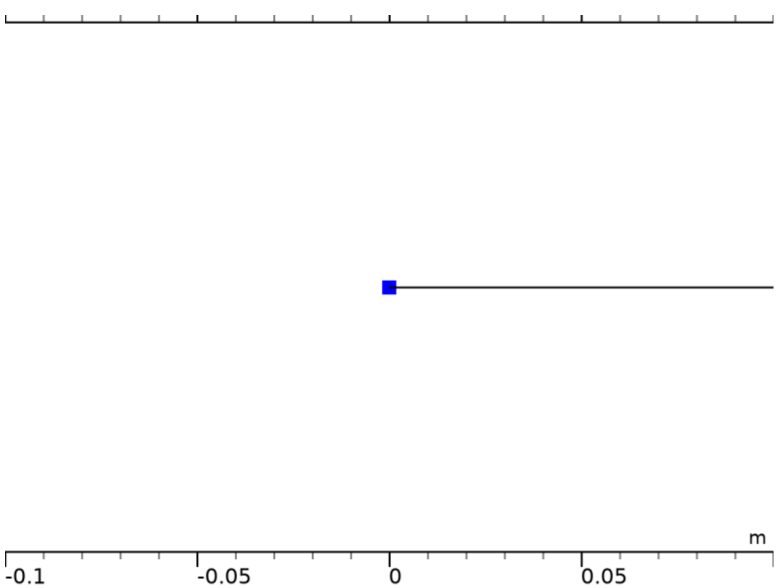

Selection

Integration 2

Coupling type	Integration
Operator name	intop2

SELECTION

Geometric entity level	Boundary
Selection	Geometry geom1: Dimension 0: Boundary 2

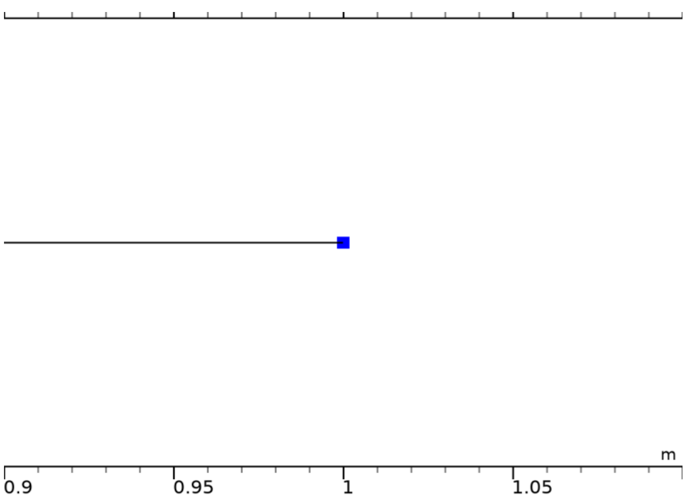

Selection

2.2 GEOMETRY 1

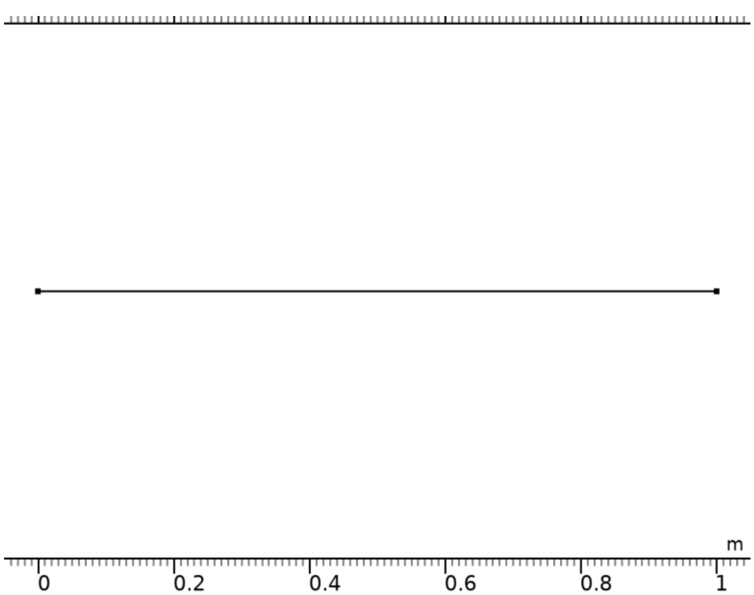

Geometry 1

UNITS

Length unit	m
Angular unit	deg

GEOMETRY STATISTICS

Description	**Value**
Space dimension	1
Number of domains	1
Number of boundaries	2

2.2.1 Interval 1 (i1)

INTERVAL

Coordinates (m)
0
1

2.3 GENERAL FORM PDE

USED PRODUCTS

COMSOL Multiphysics

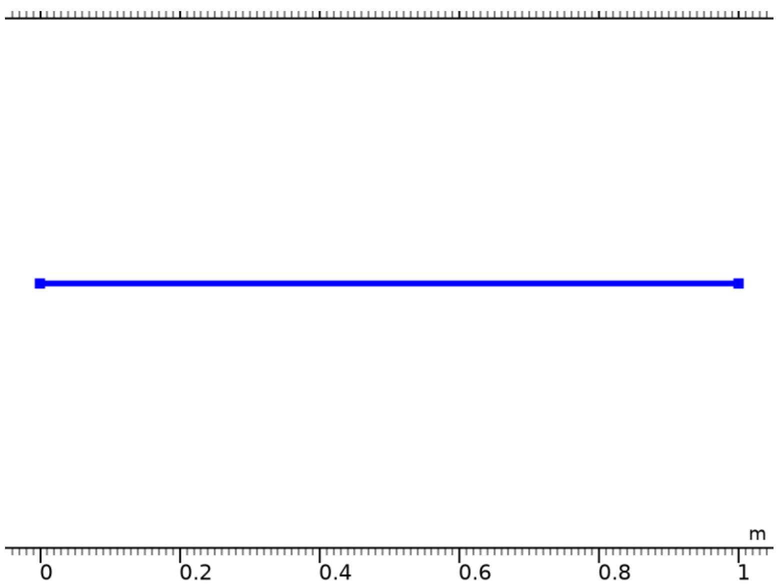

General Form PDE

SELECTION

Geometric entity level	Domain
Selection	Geometry geom1: Dimension 1: All domains

2.3.1 Interface settings

Discretization

SETTINGS

Description	Value
Shape function type	Lagrange
Element order	Quadratic
Frame	Spatial

Units

Dependent variable quantity	Unit
Dimensionless	1

Source term quantity	Unit
Custom unit	1

2.3.2 Variables

Name	Expression	Unit	Description	Selection	Details
g.nx	nx		Normal vector, x component	Boundaries 1–2	Meta
g.ny	root.ny		Normal vector, y component	Boundaries 1–2	Meta
g.nz	root.nz		Normal vector, z component	Boundaries 1–2	Meta
g.nxmesh	nxmesh		Normal vector (mesh), x component	Boundaries 1–2	Meta
g.nymesh	root.nymesh		Normal vector (mesh), y component	Boundaries 1–2	Meta
g.nzmesh	root.nzmesh		Normal vector (mesh), z component	Boundaries 1–2	Meta

2.3.3 General Form PDE 1

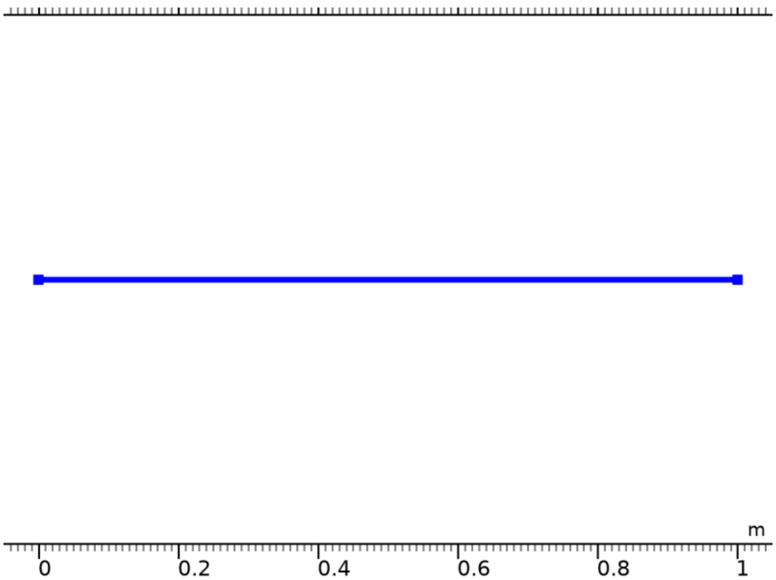

General Form PDE 1

SELECTION

Geometric entity level	Domain
Selection	Geometry geom1: Dimension 1: All domains

EQUATIONS

$$e_a \frac{\partial^2 cs}{\partial t^2} + d_a \frac{\partial cs}{\partial t} + \nabla \cdot \Gamma = f$$

$$\nabla = \frac{\partial}{\partial x}$$

SETTINGS

Description	Value
Source term	(x*lt)*d(lt, t)*csx
Conservative flux	-Ds*csx
Mass coefficient	0
Damping or mass coefficient	lt^2

Variables

Name	Expression	Unit	Description	Selection
domflux.csx	-Ds*csx	1/m	Domain flux, x component	Domain 1

Shape functions

Name	Shape function	Unit	Description	Shape frame	Selection
cs	Lagrange (Quadratic)	1	Dependent variable cs	Spatial	Domain 1

2.3.4 Zero Flux 1

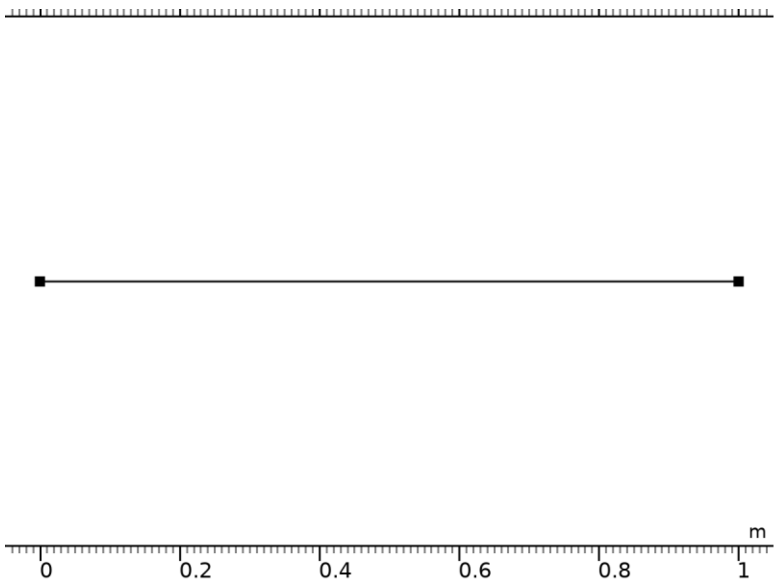

Zero Flux 1

SELECTION

Geometric entity level	Boundary
Selection	Geometry geom1: Dimension 0: All boundaries

EQUATIONS

$$-\mathbf{n}\cdot\Gamma = 0$$

2.3.5 Initial Values 1

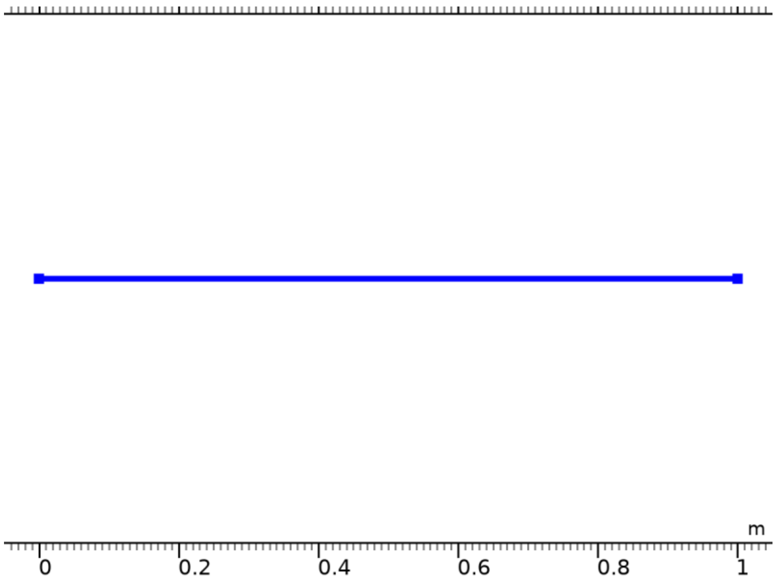

Initial Values 1

SELECTION

Geometric entity level	Domain
Selection	Geometry geom1: Dimension 1: All domains

SETTINGS

Description	Value
Initial value for cs	Ceq*epsilonSEI
Initial time derivative of cs	0

2.3.6 Dirichlet Boundary Condition 1

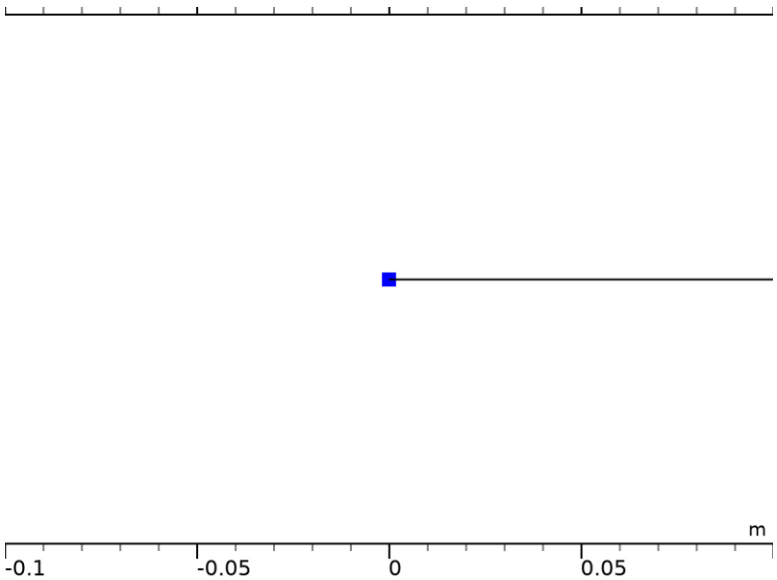

Dirichlet Boundary Condition 1

SELECTION

Geometric entity level	Boundary
Selection	Geometry geom1: Dimension 0: Boundary 1

EQUATIONS

$$cs = r$$
$$g_{\mathrm{reaction}} = -\mu$$

SETTINGS

Description	**Value**
Value on boundary	Ceq*epsilonSEI
Prescribed value of cs	On

Constraints

Constraint	**Constraint force**	**Shape function**	**Selection**	**Details**
Ceq*epsilonSEI-cs	-test(cs)	Lagrange (Quadratic)	Boundary 1	Elemental

2.3.7 Flux/Source 1

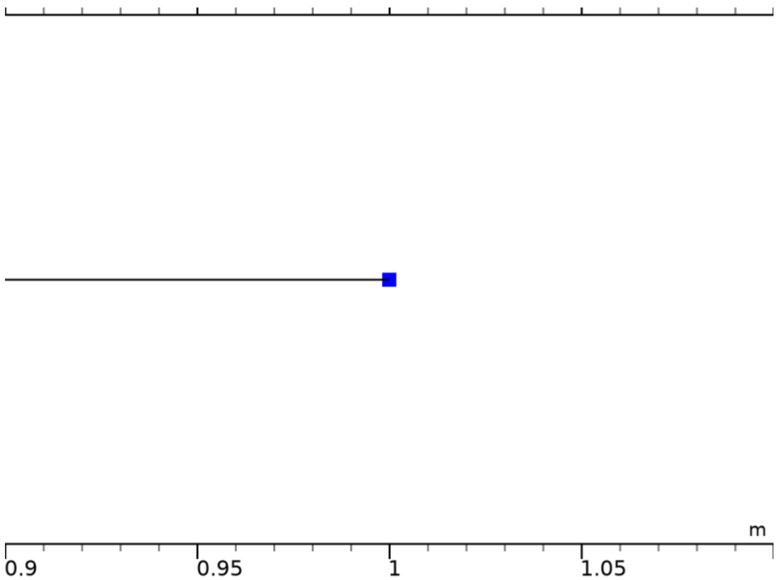

Flux/Source 1

SELECTION

Geometric entity level	Boundary
Selection	Geometry geom1: Dimension 0: Boundary 2

EQUATIONS

$$-\mathbf{n}\cdot\Gamma = g - qcs$$

SETTINGS

Description	**Value**
Boundary absorption/impedance term	0
Boundary flux/source	J_SEI/n/F*lt

Variables

Name	**Expression**	**Unit**	**Description**	**Selection**	**Details**
g.g_cs	J_SEI*lt/(n*F)	m	Boundary flux/source	Boundary 2	+ operation

2.4 GLOBAL ODES AND DAES

USED PRODUCTS

COMSOL Multiphysics

SELECTION

Geometric entity level	Entire model

2.4.1 Global Equations 1

SELECTION

Geometric entity level	Entire model

Global equations

Name	f(u,ut,utt,t)	Initial value (u_0)	Initial value (u_t0)	Description
cLi	d(cLi,t)-intop2(a*J_SEI/n/F)	xi*cLimax	0	

Units

Dependent variable quantity	Unit
Dimensionless	1

Source term quantity	Unit
Dimensionless	1

Shape functions

Name	Shape function	Unit	Description	Shape frame	Selection
cLi	ODE	1	State variable cLi		Global

2.5 GLOBAL ODES AND DAES 2

USED PRODUCTS

COMSOL Multiphysics

SELECTION

Geometric entity level	Entire model

2.5.1 Global Equations 1

SELECTION

Geometric entity level	Entire model

Global equation

Name	f(u,ut,utt,t)	Initial value (u_0)	Initial value (u_t0)	Description
lt	d(lt,t)+(intop2(Ds*csx/cp)/lt)	L0	0	

Units

Dependent variable quantity	Unit
Dimensionless	1

Source term quantity	Unit
Dimensionless	1

Shape functions

Name	Shape function	Unit	Description	Shape frame	Selection
lt	ODE	1	State variable lt		Global

2.6 OPTIMIZATION

USED PRODUCTS

COMSOL Multiphysics
Optimization Module

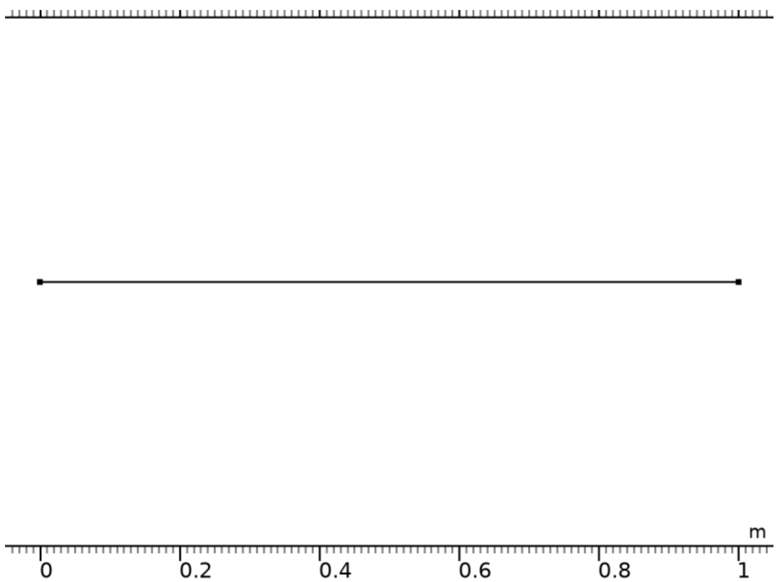

Optimization

SELECTION

Geometric entity level	Domain
Selection	Geometry geom1: Dimension 1: No domains

2.6.1 Global Least-Squares Objective 1

SELECTION

Geometric entity level	Entire model

Experimental data

SETTINGS

Description	Value
Data source	Result table
Result table	Table 1
Parameter type	Time
Time unit	d
Time column	Column 1

Use	Data column	Unit	Model expression	Weight
1	Column 2		comp1.U	1

2.7 MESH 1

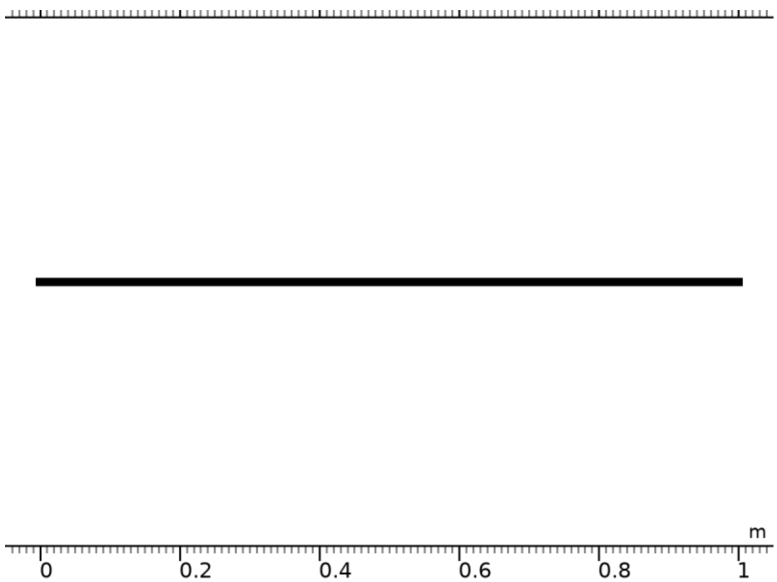

Mesh 1

2.7.1 Size (size)

SETTINGS

Description	Value
Maximum element size	0.01
Minimum element size	2.0E-5
Curvature factor	0.2
Predefined size	Extremely fine

2.7.2 Edge 1 (edg1)

SELECTION

Geometric entity level	Domain
Selection	Remaining

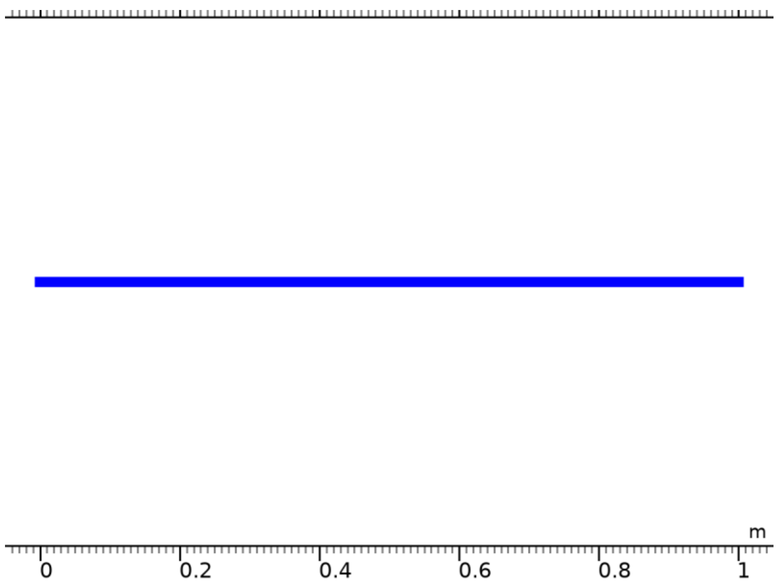

Edge 1

3 Study 1

COMPUTATION INFORMATION

Computation time	31 s
CPU	Intel64 Family 6 Model 158 Stepping 9, 4 cores
Operating system	Windows 10

3.1 OPTIMIZATION

OPTIMIZATION SOLVER

Description	Value
Method	Levenberg - Marquardt
Study step	Time Dependent

CONTROL VARIABLES AND PARAMETERS

Parameter name	Initial value	Scale	Lower bound	Upper bound
Ds0	4e-19	1e-19		
k0_SEI0	4e-17	1e-17		

MESH SELECTION

Geometry	Mesh
Geometry 1 (geom1)	nomesh

3.2 TIME DEPENDENT

Times	Unit
range(0,5,365)	d

STUDY SETTINGS

Description	Value
Include geometric nonlinearity	Off

STUDY SETTINGS

Description	Value
Time unit	d
Times	{0, 5, 10, 15, 20, 25, 30, 35, 40, 45, 50, 55, 60, 65, 70, 75, 80, 85, 90, 95, 100, 105, 110, 115, 120, 125, 130, 135, 140, 145, 150, 155, 160, 165, 170, 175, 180, 185, 190, 195, 200, 205, 210, 215, 220, 225, 230, 235, 240, 245, 250, 255, 260, 265, 270, 275, 280, 285, 290, 295, 300, 305, 310, 315, 320, 325, 330, 335, 340, 345, 350, 355, 360, 365}

PHYSICS AND VARIABLES SELECTION

Physics interface	Discretization
General Form PDE (g)	physics
Global ODEs and DAEs (ge)	physics
Global ODEs and DAEs 2 (ge2)	physics
Optimization (opt)	physics

MESH SELECTION

Geometry	Mesh
Geometry 1 (geom1)	mesh1

3.3 SOLVER CONFIGURATIONS

3.3.1 Solution 1

Compile Equations: Time Dependent (st1)

STUDY AND STEP

Description	Value
Use study	Study 1
Use study step	Time Dependent

Dependent Variables 1 (v1)

GENERAL

Description	**Value**
Defined by study step	Time Dependent

RESIDUAL SCALING

Description	**Value**
Method	Manual

INITIAL VALUE CALCULATION CONSTANTS

Constant name	**Initial value source**
t	range(0,5,365)
timestep	0.365[d]

Dependent variable cs (comp1.cs) (comp1_cs)

GENERAL

Description	**Value**
Field components	comp1.cs
Internal variables	{comp1.uflux.cs, comp1.dflux.cs}

Control parameter Ds0 (conpar2) (conpar2)

GENERAL

Description	**Value**
State components	Ds0

SCALING

Description	**Value**
Method	Manual
Scale	1.0E-19

Control parameter k0_SEI0 (conpar4) (conpar4)

GENERAL

Description	Value
State components	k0_SEI0

SCALING

Description	Value
Method	Manual
Scale	1.0E-17

State variable cLi (comp1.ODE1) (comp1_ODE1)

GENERAL

Description	Value
State components	comp1.cLi

State variable lt (comp1.ODE2) (comp1_ODE2)

GENERAL

Description	Value
State components	comp1.lt

Optimization Solver 1 (o1)

GENERAL

Description	Value
Defined by study step	Optimization

OPTIMIZATION SOLVER

Description	Value
Method	Levenberg - Marquardt

RESULTS WHILE SOLVING

Description	Value
Plot	On

Description	Value
Plot group	1D Plot Group 4

Time-Dependent Solver 1 (t1)

GENERAL

Description	Value
Defined by study step	Time Dependent
Time unit	d
Times	{0, 5, 10, 15, 20, 25, 30, 35, 40, 45, 50, 55, 60, 65, 70, 75, 80, 85, 90, 95, 100, 105, 110, 115, 120, 125, 130, 135, 140, 145, 150, 155, 160, 165, 170, 175, 180, 185, 190, 195, 200, 205, 210, 215, 220, 225, 230, 235, 240, 245, 250, 255, 260, 265, 270, 275, 280, 285, 290, 295, 300, 305, 310, 315, 320, 325, 330, 335, 340, 345, 350, 355, 360, 365}

RESULTS WHILE SOLVING

Description	Value
Probes	None

LEAST-SQUARES DATA

Description	Value
Times	{166834.68360398075, 168731.8004075036, 353086.91566755227, 476511.1030026704, 849461.9475541757, 1159361.5571650453, 1406656.3122596391, 1903031.3441462629, 2523165.3486862713, 2894888.647070791, 3391040.4887452326, 3701163.2885682806, 4197761.510667083, 4880835.155041638, 5191181.145076865, 5439368.661020178, 6060060.641090635, 6494723.579309699, 7177908.818790341, 7861094.058270985, 8606437.771843547, 9414051.554614116, 9973143.036123103, 1.0843138483197767E7, 1.1526323722678414E7, 1.2582906187134914E7, 1.3452566848891312E7, 1.4446990839255903E7, 1.500619391587098E7, 1.5565396992486056E7, 1.618675854319305E7, 1.693232544697779E7, 1.774027401506663E7, 1.836163556577362E7, 1.9107425659770545E7, 1.9604358667187616E7, 2.041219564017036E7, 2.1033557190877356E7, 2.1530824983612694E7, 2.2276503482503522E7, 2.3022181981394358E7, 2.376808367049737E7, 2.4762619255968045E7, 2.544625087587304E7, 2.5756708461014368E7, 2.6377846821509182E7, 2.7061143656095907E7, 2.7496252974739335E7, 2.8179772999538247E7, 2.8738976076153323E7, 2.948443138483198E7, 2.9794777374867205E7,

Description	Value
	3.0229886693510633E7, 3.0851136649111153E7, 3.1223975898556944E7}
Least-squares times from file	1.67e+05 1.69e+05 3.53e+05 4.77e+05 8.49e+05 1.16e+06 1.41e+06 1.90e+06 2.52e+06 2.89e+06 3.39e+06 3.70e+06 4.20e+06 4.88e+06 5.19e+06 5.44e+06 6.06e+06 6.49e+06 7.18e+06 7.86e+06 8.61e+06 9.41e+06 9.97e+06 1.08e+07 1.15e+07 1.26e+07 1.35e+07 1.44e+07 1.50e+07 1.56e+07 1.62e+07 1.69e+07 1.77e+07 1.84e+07 1.91e+07 1.96e+07 2.04e+07 2.10e+07 2.15e+07 2.23e+07 2.30e+07 2.38e+07 2.48e+07 2.54e+07 2.58e+07 2.64e+07 2.71e+07 2.75e+07 2.82e+07 2.87e+07 2.95e+07 2.98e+07 3.02e+07 3.09e+07 3.12e+07

Fully Coupled 1 (fc1)

GENERAL

Description	Value
Linear solver	Direct

4 Results

4.1 DATASETS

4.1.1 Study 1/Solution 1

SOLUTION

Description	Value
Solution	Solution 1
Component	Save Point Geometry 1

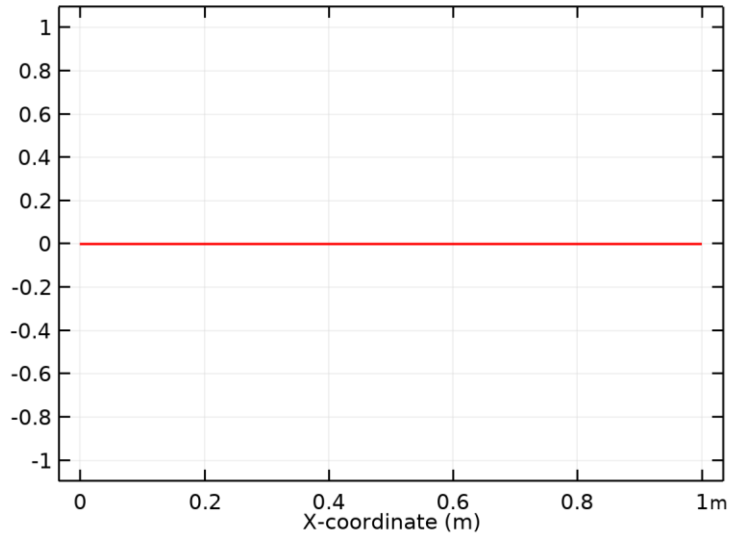

Dataset: Study 1/Solution 1

4.2 DERIVED VALUES

4.2.1 Global Evaluation 1

DATA

Description	**Value**
Dataset	Study 1/Solution 1

EXPRESSIONS

Expression	**Unit**	**Description**
cLi	1	State variable cLi

4.2.2 Global Evaluation 2

DATA

Description	**Value**
Dataset	Study 1/Solution 1

EXPRESSIONS

Expression	**Unit**	**Description**
lt	1	State variable lt

4.3 TABLES

4.3.1 Table 1

Column 1	Column 2
1.9310	0.048520
1.9529	0.052027
4.0867	0.058165
5.5152	0.060749
9.8317	0.060746
13.419	0.063328
16.281	0.067204
22.026	0.069784
29.203	0.073979
33.506	0.077531
39.248	0.080758
42.838	0.082694
48.585	0.084628
56.491	0.086561
60.083	0.087850
62.956	0.089141
70.140	0.091720
75.170	0.093009
83.078	0.094618
90.985	0.096228
99.612	0.097836
108.96	0.099121
115.43	0.10009
125.50	0.10072
133.41	0.10233
145.64	0.10265
155.70	0.10425
167.21	0.10457
173.68	0.10521
180.16	0.10585
187.35	0.10649
195.98	0.10745
205.33	0.10777
212.52	0.10841
221.15	0.10873
226.90	0.10969
236.25	0.11033
243.44	0.11097
249.20	0.11097
257.83	0.11160

Column 1	Column 2
266.46	0.11224
275.09	0.11224
286.60	0.11223
294.52	0.11254
298.11	0.11351
305.30	0.11480
313.21	0.11608
318.24	0.11608
326.15	0.11672
332.63	0.11736
341.25	0.11865
344.85	0.11994
349.88	0.11993
357.07	0.12090
361.39	0.12122

4.3.2 Objective Probe Table 2

Iteration number	Objective
1.0000	1.0525E-4
2.0000	9.8185E-5
3.0000	9.1829E-5
4.0000	9.0184E-5
5.0000	8.1913E-5
6.0000	8.1899E-5
7.0000	8.1899E-5

4.3.3 Confidence Intervals Table 3

Parameter value	Variance	Standard deviation	Confidence (+/-)
1.4029E-19	4.7588E-40	2.1815E-20	4.3755E-20
1.6434E-17	4.6872E-36	2.1650E-18	4.3424E-18

4.4 PLOT GROUPS

4.4.1 1D Plot Group 1

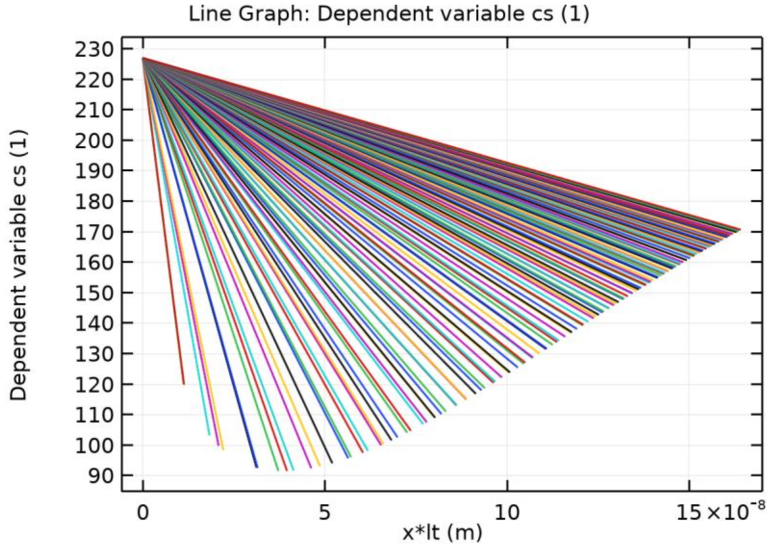

Line Graph: Dependent variable cs (1)

4.4.2 1D Plot Group 2

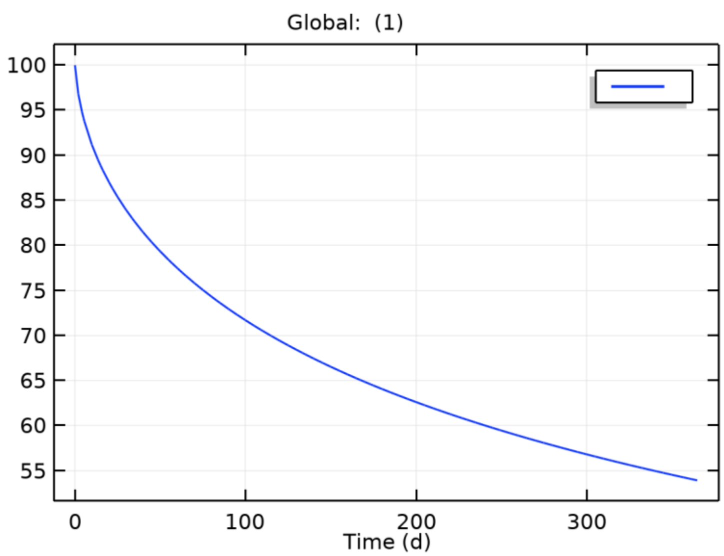

Global: (1)

4.4.3 1D Plot Group 3

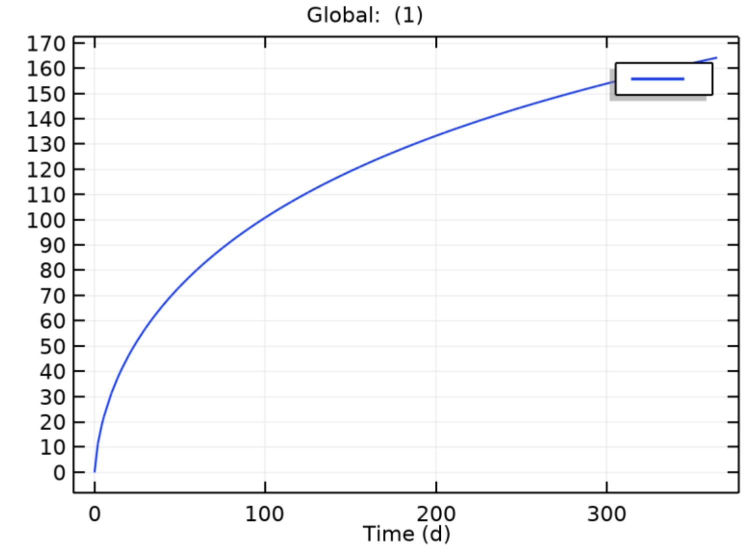

Global: (1)

4.4.4 1D Plot Group 4

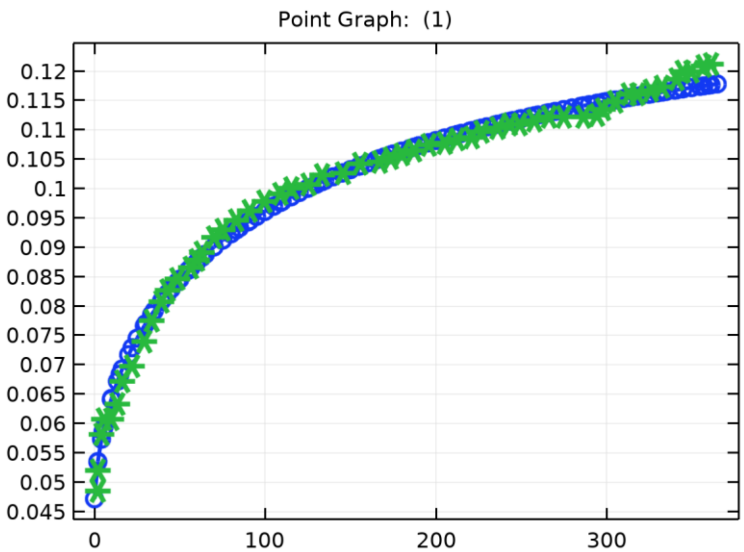

Point Graph: (1)

APPENDIX D

COMPUTATION IN MATLAB

Finite difference method is numerically solved by MATLAB. We discrete a domain into several elements so that there is an ordinary differential equation in every element. Making it easier to simulate and getting estimated parameters with experimental data. The MATLAB codes are shown below.

MATLAB Code:

```
clc
clearvars
clear all;
close all
format short g
tic
global xbest Fobjbest ii
Fobjbest =1e5;
iter= 0;
%            D(1)        k(2)
x0     = log([1e-21       1e-17]);
lb     = log([1e-22       1e-20]);
ub     = log([1e-16       1e-13]);
```

```
% options      = optimset('display','iter','MaxFunEvals',1000,'TolX',1e-2,'MaxIter',20);
% options = optimset('Display','iter','TolFun',1e-12,'MaxIter',100,'TolX',1e-
16,'FinDiffRelStep',1e-16,'MaxFunEvals',300);
% options = optimset('Display','iter','TolFun',1e-12,'MaxIter',50,'TolX',1e-
12,'MaxFunEvals',200,'FinDiffRelStep',1e-16);
% options = optimoptions('lsqnonlin','Display','iter','OptimalityTolerance', 1e-
10,'StepTolerance', 1e-10,'FunctionTolerance', 1e-10);
% options      = optimset('display','iter','MaxFunEvals',1000,'TolX',1e-
3,'FinDiffRelStep',1e-2,'MaxIter',10);
options= optimset('display','iter','MaxFunEvals',1000,'TolFun',1.e-12,'TolX',1e-
12,'FinDiffRelStep',1e-8,'MaxIter',200);
% options=optimset('MaxIter',200,'TolFun',1.e-10,'TolX',1.e-10,'Algorithm','trust-region-
reflective',...
%'MaxFunEvals',200,'Display','iter');
[x,resnorm,residual,exitflag,output,lambda,jacobian] =
lsqnonlin(@ObjFunc,x0,lb,ub,options);
x= exp(x)
% J=full(jacobian);
% residual=(residual)';
% CI=ParaCI(x',residual,J,0.95);
RunE = load('OCV experimental.txt');
tData            = RunE(:,1);
OCV_data       = RunE(:,2);
```

```
[tModel, Curr_mod] = Main_FDM(x(1),x(2));

toc

%% PLOT EXP and SIM Results

figure()

plot(tData,OCV_data,'ob',tModel,Curr_mod,'-r','linewidth',2)

xlabel('time d','fontsize',16)

ylabel('OCV V','fontsize',16)

legend('Experimental','Model')

title(['D = ' num2str(x(1)) ,' k = ' num2str(x(2))],'fontsize',16)


function [tmodel, Ocvmodel] = Main_FDM(D,k)

%% parameters

p.Ds0= D;

p.k0_SEI0 = k;

p.Ceq = 4541;

p.cp= 28556;

p.L0= 1e-12;

p.F = 96485;

p.U_SEI=; 0.4

p.R= 8.3145;

p.T = 298.15;

p.epsilonSEI = 0.05;

p.n= 2;
```

```
p.a= 3e6;

p.cLimax= 3.056e4;

p.cs0= p.Ceq*p.epsilonSEI;

p.n_tot= 100;

p.h= 1/(p.n_tot-1);

p.Ds= p.Ds0;

p.k0_SEI= p.k0_SEI0;

p.csmax= p.Ceq;


%% IC's and mass matrix

y0= [p.cs0*ones(1,p.n_tot),p.cLimax,p.L0];

M= eye(p.n_tot+2,p.n_tot+2);

M(1,1) = 0;

M(p.n_tot,p.n_tot)=0;

% tsp= 3600*365*24;

% tspan= [0:3600*24*3:tsp];

RunE= load('OCV experimental.txt');

tspan= 3600*24*RunE(:,1);

options = odeset('Mass',M, 'RelTol', 1e-10,'AbsTol', 1e-10);

[t,Y]= ode15s(@(t,y) MBEQS(t,y,p),tspan,y0,options);

%% post processing

tmodel       = t/3600/24;

Ocvmodel    = Un(Y(:,p.n_tot+1)/p.cLimax);
```

```
% figure()

% plot(tmodel,Ocvmodel,'LineWidth',2);

% hold all;

% exp= load('OCV experimental.txt');

% texp= exp(:,1)';

% yexp= exp(:,2:end)';

% plot(texp,yexp,'o','LineWidth',2,'color','r')

% legend('FDM Matlab','Experimental')

end


function [eqs]= MBEQS(t,y,p)

soc_N= y(p.n_tot+1)/p.cLimax;

U= Un(soc_N);

eta_SEI= U-p.U_SEI;

J_SEI= -p.n*p.F*p.k0_SEI*y(p.n_tot)*soc_N^2*exp(-0.5*p.F*eta_SEI*p.n/p.R/p.T);

dldt= (-(p.Ds/y(p.n_tot+2)/p.cp)*(3*y(p.n_tot)-4*y(p.n_tot-1)+y(p.n_tot-2))/2/p.h);

dydt(1) = y(1)-p.cs0;

for i=2:p.n_tot-1

dydt(i)= p.Ds*(y(i-1)-2*y(i)+y(i+1))/(y(p.n_tot+2)*p.h)^2 +((i-

1)/y(p.n_tot+2))*dldt*(y(i-1)-y(i+1))/2;

end

dydt(p.n_tot)= (3*y(p.n_tot) - 4*y(p.n_tot-1) + y(p.n_tot-2))/(2*p.h) -

J_SEI*y(p.n_tot+2)/(p.Ds*p.n*p.F);
```

```
dydt(p.n_tot+1) = p.a*J_SEI/p.n/p.F;

dydt(p.n_tot+2) = -(p.Ds/y(p.n_tot+2)/p.cp)*(3*y(p.n_tot)-4*y(p.n_tot-1)+y(p.n_tot-
2))/2/p.h;

eqs= dydt';

end


function ResT = ObjFunc(x)

global xbest Fobjbest

D= exp(x(1));

k= exp(x(2));

%% Run COMSOL Model

[t, Ocvmodel] = Main_FDM(D,k);


%% Load SIMULATION Results

tModel= t;

OCV_mod= Ocvmodel;

%% Load EXPERIMENTAL Data

RunE= load('OCV experimental.txt');

tData= 3600*24*RunE(:,1);

OCV_data= RunE(:,2);

% OCV_exp= @(t)spline(tData,OCV_data,t);

% OCVexp= OCV_exp(tModel);

%% Calculate RESIDUALS

Res= (OCV_mod-OCV_data);
```

```
ResT= Res(:);

Fobj= sum(ResT.^2);

if Fobj<Fobjbest

xbest= x;

Fobjbest = Fobj;

save('last_res','xbest','Fobjbest')

end

end
```

MATLAB result: